

---

ETD Archive

---

2011

## Characterization of Elastin-Like Polypeptides Using Viscometry

Hamdan Noman Alanazi  
*Cleveland State University*

Follow this and additional works at: <https://engagedscholarship.csuohio.edu/etdarchive>

 Part of the [Biomedical Engineering and Bioengineering Commons](#)

**How does access to this work benefit you? Let us know!**

---

### Recommended Citation

Alanazi, Hamdan Noman, "Characterization of Elastin-Like Polypeptides Using Viscometry" (2011). *ETD Archive*. 463.  
<https://engagedscholarship.csuohio.edu/etdarchive/463>

This Thesis is brought to you for free and open access by EngagedScholarship@CSU. It has been accepted for inclusion in ETD Archive by an authorized administrator of EngagedScholarship@CSU. For more information, please contact [library.es@csuohio.edu](mailto:library.es@csuohio.edu).

CHARACTERIZATION OF ELASTIN-LIKE POLYPEPTIDES USING  
VISCOMETRY

HAMDAN ALANAZI

Bachelor of Science in Chemical Engineering

Cleveland State University

May, 2010

submitted in partial fulfillment of requirements for the degree

MASTER OF SCIENCE IN CHEMICAL ENGINEERING

at the

CLEVELAND STATE UNIVERSITY

July, 2011

This thesis has been approved for the Department of Chemical and Biomedical Engineering and the College of Graduate Studies by

---

Dr. Nolan B. Holland  
Department of Chemical and Biomedical Engineering  
Cleveland State University

---

Date

---

Dr. Orhan Talu  
Department of Chemical and Biomedical Engineering  
Cleveland State University

---

Date

---

Dr. Dhananjai B. Shah  
Department of Chemical and Biomedical Engineering  
Cleveland State University

---

Date

## **ACKNOWLEDGMENTS**

I would like to express my sincere gratitude to my academic advisor Dr. Nolan B. Holland for the research opportunity that he provided me at his laboratory. He taught me valuable lessons and his continuous support, patience, encouragement, and guidance are invaluable appreciated.

I would also like to extend my regards to my committee members Dr. Dhananjai B. Shah and Dr. Orhan Talu for their valuable support and advices. Thanks also go out to the faculty and the staff of the Chemical Engineering Department at Cleveland State University for the family atmosphere that I and many other international students are experiencing on a daily basis. Special thanks are paid to Ms. Becky Laird and Darlene Montgomery for their continuous support throughout my stay at Cleveland State University.

My colleagues at the laboratory were always supportive and I would like to gratefully thank them. Thank you to Ali Ghoorchian for providing me some of the ELPs and also for his support and advice.

I would like also to acknowledge The Saudi Arabian Ministry of Higher Education and The Saudi Cultural Mission at the United States for their generous support. This work has been supported by the National Science Foundation (DMR-0908795).

Finally, I would like to sincerely and gratefully thank my parents and my family for their great love and support. Thank you to my friends and specially those who encouraged me and supported me throughout the completion of my academic career.

# CHARACTERIZATION OF ELASTIN-LIKE POLYPEPTIDES USING VISCOMETRY

HAMDAN ALANAZI

## ABSTRACT

Elastin-like polypeptides (ELPs) are a class of polypeptide polymers that are gaining interest in various potential applications. These polymers are responsive to the changes in their environment by exhibiting conformational changes and aggregation. Monodisperse elastin-like polypeptides, (GVGVP)<sub>40</sub>, (GVGVP)<sub>40</sub>-foldon, and (GVGVP)<sub>60</sub>-foldon are made in bacterial expression system. An Ubbelohde capillary viscometer was set up to characterize the structural changes of these ELPs in phosphate buffered saline (PBS) solution. For the ELP-foldon, the relative viscosity measurements were utilized to calculate the intrinsic viscosities using Kraemer and Huggins equations. The known molecular weights of the ELPs and the experimentally determined intrinsic viscosities facilitated the calculation of the Mark-Houwink-Sakurada constants. The value of the exponential  $a$  in the Mark-Houwink-Sakurada equation was 0.69 at 20°C and it decreased as the temperature increased until it reached 0.51 at 26°C. The observed changes in  $a$  indicate that the conformation of the polymer coils changes from expanded and hydrated coils to theta coils. Viscosity measurements were limited in this project by concentration, since low concentrations produced small specific viscosities with large errors. A second limitation on the viscosity measurements was the aggregation of the polymers. The polymers aggregated at their phase transition temperature,  $T_i$ , and they phase separated.

## TABLE OF CONTENTS

	Page
ABSTRACT.....	iv
LIST OF TABLES.....	vii
LIST OF FIGURES.....	viii
 CHAPTER	
I. INTRODUCTION AND BACKGROUND.....	1
1.1 Introduction.....	1
1.1.1 Elastin-Like Polypeptides (ELPs).....	2
1.1.2 ELPs Applications.....	5
1.2 ELPs Temperature Dependence ( $T_t$ ).....	6
1.3 Factors Impacting the Transition Temperature ( $T_t$ ).....	8
1.3.1 Salt Concentration.....	8
1.3.2 The pH Level.....	11
1.3.3 Chain Length and Concentration.....	13
1.4 Structural Changes of ELPs.....	16
1.5 Characterization of ELPs.....	19
1.5.1 Biophysical Properties Characterization.....	19
1.5.2 Structural Properties Characterization.....	20
1.5.3 Bulk Properties Characterization.....	20
1.6 Polymer Characterization Using Capillary Viscometer.....	21
1.6.1 Viscosity.....	21

1.6.2 Mark-Houwink-Sakurada (MHS) Constants and ELPs	
Conformation.....	23
1.6.3 Sphere Equivalent Radius of ELPs.....	24
II. MATERIALS AND METHOD.....	26
2.1 Overview.....	26
2.2 ELPs Expression and Purification.....	26
2.2.1 Media Preparation.....	27
2.2.2 Starting the Culture.....	28
2.2.3 Sonication.....	28
2.2.4 Purification.....	29
2.3 Concentration Measurements.....	29
2.4 Verifying the Viscometer Calibration.....	29
2.5 Viscosity Measurements.....	31
III. RESULTS AND DISCUSSION.....	33
3.1 Viscosity Calculations and Analysis.....	33
3.2 Temperature Dependent ELP Conformational Changes.....	37
3.3 Interpretation of Mark-Houwink-Sakurada (MHS) Constants.....	40
IV. CONCLUSIONS.....	43
BIBLIOGRAPHY.....	45
APPENDICES.....	53
A. Viscometer Constant Calibration.....	54
B. Intrinsic Viscosity Graphs.....	55
C. Viscosity Measurements Procedure.....	62

## LIST OF TABLES

Table	Page
1.1 Proteins–Based Polymers Advantages.....	2
1.2 The Codons of the 20 Amino Acids.....	4
1.3 The Effects of Guest Residue on the $T_t$ .....	15
1.4 Geometrical Interpretations of Mark-Houwink-Sakurada exponent $a$ .....	24
2.1 ELPs Amino Acid Sequences and Molecular Weights.....	27
3.1 Experimental Values of Mark-Houwink-Sakurada constant $a$ .....	42



## LIST OF FIGURES

Figure	Page
1.1 A Dipeptide from Two Alpha Amino Acids.....	3
1.2 A Schematic of Lower Critical Solution Temperature (LCST).....	6
1.3 Water Ratio in Poly(GVGVP) as Function of Temperature.....	7
1.4 Influence of Salt Concentration on $T_i$ for (GVGVP) <sub>251</sub> .....	9
1.5 Influence of Salt Concentration on $T_i$ for Poly(GVGVP)-foldon.....	10
1.6 ELP Phase Behavior Dependence on pH and Concentration.....	12
1.7 Influence of Concentration on $T_i$ for ELP(V <sub>5</sub> A <sub>2</sub> G <sub>3</sub> ).....	13
1.8 Influences of Concentration and Chain Length on $T_t$ .....	14
1.9 Equilibrium Weight Swelling Ratios of Pentapeptides.....	18
1.10 Influence of the Molar Concentration of Poly(GVGVP) on $T_t$ .....	19
1.11 A Schematic of the Effect of Shear Rate on the Polymer Chain Rotation.....	21
1.12 The Equivalent Sphere Model.....	25
2.1 Viscometry Bath with a Heating Circulator.....	30
2.2 Schematic Drawing of Cannon Capillary Viscometer.....	31
2.3 Clear and Turbid Solutions of Poly(GVGVP)-foldon.....	32
3.1 The Kinematic Viscosity of PBS and Different ELPs.....	34
3.2 Plot of $\eta_{\text{specific}}/c$ and $\ln \eta_{\text{relative}}/c$ versus $c$ for (GVGVP) <sub>40</sub> -foldon extrapolated to zero concentration at 20°C.....	35
3.3 The Intrinsic Viscosities for (GVGVP) <sub>40</sub> -foldon and (GVGVP) <sub>60</sub> -foldon as Function of Temperature.....	37
3.4 Random Coil Polymer Transition as Function of Temperature.....	38
3.5 The Folding of the Three-Armed Star Polymer.....	38

3.6	Sphere Equivalent Volume of (GVGVP) <sub>40</sub> -foldon and (GVGVP) <sub>60</sub> -foldon as Function of Temperature.....	39
3.7	Log $[\eta]$ of versus Log MW for (GVGVP) <sub>60</sub> -foldon and (GVGVP) <sub>40</sub> -foldon.....	41
A.1	Viscosity of Water and PBS Solvent.....	54
B.1	Plot of $\eta_{\text{specific}}/c$ and $\ln \eta_{\text{relative}}/c$ versus $c$ for (GVGVP) <sub>40</sub> -foldon extrapolated to zero concentration at 20°C.....	55
B.2	Plot of $\eta_{\text{specific}}/c$ and $\ln \eta_{\text{relative}}/c$ versus $c$ for (GVGVP) <sub>40</sub> -foldon extrapolated to zero concentration at 21°C.....	55
B.3	Plot of $\eta_{\text{specific}}/c$ and $\ln \eta_{\text{relative}}/c$ versus $c$ for (GVGVP) <sub>40</sub> -foldon extrapolated to zero concentration at 22°C.....	56
B.4	Plot of $\eta_{\text{specific}}/c$ and $\ln \eta_{\text{relative}}/c$ versus $c$ for (GVGVP) <sub>40</sub> -foldon extrapolated to zero concentration at 23°C.....	56
B.5	Plot of $\eta_{\text{specific}}/c$ and $\ln \eta_{\text{relative}}/c$ versus $c$ for (GVGVP) <sub>40</sub> -foldon extrapolated to zero concentration at 24°C.....	57
B.6	Plot of $\eta_{\text{specific}}/c$ and $\ln \eta_{\text{relative}}/c$ versus $c$ for (GVGVP) <sub>40</sub> -foldon extrapolated to zero concentration at 25°C.....	57
B.7	Plot of $\eta_{\text{specific}}/c$ and $\ln \eta_{\text{relative}}/c$ versus $c$ for (GVGVP) <sub>60</sub> -foldon extrapolated to zero concentration at 20°C.....	58
B.8	Plot of $\eta_{\text{specific}}/c$ and $\ln \eta_{\text{relative}}/c$ versus $c$ for (GVGVP) <sub>60</sub> -foldon extrapolated to zero concentration at 21°C.....	58
B.9	Plot of $\eta_{\text{specific}}/c$ and $\ln \eta_{\text{relative}}/c$ versus $c$ for (GVGVP) <sub>60</sub> -foldon extrapolated to zero concentration at 22°C.....	59

B.10	Plot of $\eta_{\text{specific}}/c$ and $\ln \eta_{\text{relative}}/c$ versus $c$ for (GVGVP) <sub>60</sub> -foldon extrapolated to zero concentration at 23°C.....	59
B.11	Plot of $\eta_{\text{specific}}/c$ and $\ln \eta_{\text{relative}}/c$ versus $c$ for (GVGVP) <sub>60</sub> -foldon extrapolated to zero concentration at 24°C.....	60
B.12	Plot of $\eta_{\text{specific}}/c$ and $\ln \eta_{\text{relative}}/c$ versus $c$ for (GVGVP) <sub>60</sub> -foldon extrapolated to zero concentration at 25°C.....	60
B.13	Plot of $\eta_{\text{specific}}/c$ and $\ln \eta_{\text{relative}}/c$ versus $c$ for (GVGVP) <sub>40</sub> extrapolated to zero concentration at 25°C.....	61
B.14	Plot of $\eta_{\text{specific}}/c$ and $\ln \eta_{\text{relative}}/c$ versus $c$ for (GVGVP) <sub>40</sub> extrapolated to zero concentration at 30°C.....	61

## CHAPTER I

### INTRODUCTION AND BACKGROUND

#### 1.1 Introduction

In the last two decades, research in protein-based polymers, i.e. polymers that are based on protein sequences, has been increasing. Protein-based polymers can be synthesized chemically or by recombinant DNA technology [1]. The later is better for the preparation of the protein-based polymer in large-scale production. The usage of the DNA technology also gives precise control of the molecular weight, amino acids sequence, and stereochemistry. Protein-based polymers have several advantages over petroleum-based polymers and summary of those advantages are listed in Table 1.1.

**Table 1.1: General advantages of protein –based polymers over conventional polymers** (Modified from reference [2])

---

1. There are two synthetic approaches to produce protein-based polymers, chemical or encoding in DNA.
2. When using the DNA technology, there is a possibility of the selection of 20 different amino acids that give the flexibility of selecting from a range of monomers.
3. Precise sequence of the monomers can be obtained using the recombinant DNA technology.
4. Precise control of the stereochemistry and therefore the structural and the physical properties of the polymer.
5. The protein-based polymers from a single gene have the same chain lengths.
6. They have the capacity to mimic the structures and the functions of biological proteins.
7. They can be produced and disposed in an environment friendly manner.

The variety of protein-based polymers designs using 20 amino acids inspired many studies of ELPs such as poly(GVGVP) and its modified polymers [3]. The letter G represents glycine while V stands for valine and P stands for proline. The sequence of the amino acids in poly(GVGVP) has been found in tropoelastin, which is the precursor protein to the elastin molecule that is responsible for the resilience of tissues [4,5]. The temperature induced conformational changes of ELPs are investigated in this project using viscosity measurements.

#### 1.1.1 Elastin-Like Polypeptides (ELPs)

Elastin is a protein that has an elastic recoil property and can be found in blood vessels, lungs, and skin. It consists of repeating hydrophobic and hydrophilic cross-linking domains. Proline, valine, alanine and leucine are the dominant hydrophobic

amino acids while the cross-linking domain contains lysyl residues in addition to proline rich regions or polyalanine. The synthesis of elastin requires the synthesis of a precursor protein called tropoelastin. Tropoelastin and elastin-like polypeptides (ELPs) can go into an organized self-assembled structure. The temperature-induced structure is reversible and known as coacervation [6,7].

ELPs are a class of polypeptides that is inspired by the amino acid sequence in elastin. They are responsive materials that exhibit conformational changes and aggregation due to their sensitivity to slight changes in the surrounding environment such as changes in temperature, pH level, light or a combination of different environmental triggers. The peptide structure needs to be discussed to understand the structure of ELPs. A polypeptide is a linear polymer and it is built by amino acids (Figure 1.1) [8]. The side chain (R) at the  $\alpha$  carbon, the carbon attaching the amino group ( $-NH_2$ ) and carboxylic group ( $-COOH$ ) groups, differentiates between the various amino acids. A chain of peptide always has an amino group at one end (N-terminal) and a carboxyl group at the other end (C-terminal).

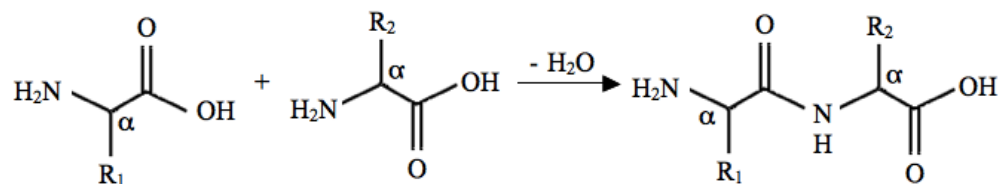


**Figure 1.1: Formation of a dipeptide from two alpha amino acids** (Modified from reference [8])

Information from genes can be converted into proteins through the genetic coding. An amino acid can be represented by a specific codon of three consecutive nucleotides (Table 1.2).

**Table 1.2: The 20 amino acids and their corresponding abbreviations and codons**  
(Modified from reference [8])

Amino Acids	Abbreviations		Codons
Alanine	Ala	<b>A</b>	GCA GCC GCG GCU
Cysteine	Cys	<b>C</b>	UGC UGU
Aspartic acid	Asp	<b>D</b>	GAC GAU
Glutamic acid	Glu	<b>E</b>	GAA GAG
Phenylalanine	Phe	<b>F</b>	UUC UUU
Glycine	Gly	<b>G</b>	GGA GGC GGG GGU
Histidine	His	<b>H</b>	CAC CAU
Isoleucine	Ile	<b>I</b>	AUA AUC AUU
Lysine	Lys	<b>K</b>	AAA AAG UUA UUG CUA CUC CUG
Leucine	Leu	<b>L</b>	CUU
Methionine	Met	<b>M</b>	AUG
Asparagine	Asn	<b>N</b>	AAC AAU
Proline	Pro	<b>P</b>	CCA CCC CCG CCU
Glutamine	Gln	<b>Q</b>	CAA CAG AGA AGG CGA CGC CGG
Arginine	Arg	<b>R</b>	CGU AGC AGU UCA UCC UCG
Serine	Ser	<b>S</b>	UCU
Threonine	Thr	<b>T</b>	ACA ACC ACG ACU
Valine	Val	<b>V</b>	GUA GUC GUG GUU
Tryptophan	Trp	<b>W</b>	UGG
Tyrosine	Tyr	<b>Y</b>	UAC UAU

The artificial ELPs that are being studied in this project are encoded in DNA and produced in bacterial expression systems. The fundamental repeat unit of the ELP is  $(G\alpha G\beta P)_n$  where  $\alpha$  and  $\beta$  could be any of the amino acids with the exception of proline for  $\beta$  and  $n$  is the number of the repeated blocks. Three ELPs,  $(GVGVP)_{40}$ ,  $(GVGVP)_{40}$ -foldon and  $(GVGVP)_{60}$ -foldon, were utilized for this project. One of their most critical properties is that they are soluble in aqueous solutions below their transition temperature,  $T_t$ , and they quickly aggregate above their  $T_t$ . The aggregation of ELPs is useful in many applications such as purifying them by separating the aggregate from the contaminants using centrifugation above the  $T_t$  [9].

### 1.1.2 ELPs Applications

The responsiveness of the ELPs makes them suitable for applications in engineering, pharmaceutical, and biomedical sciences [10-13]. The structural controls of the ELPs via the DNA encoding synthesis make them valuable for many biomedical applications. The sequence of the polypeptide can be controlled to target specific types, numbers, and locations of any reactive sites. The half-life of the ELPs *in vivo* and their degradation in animal bodies are dependent on their molecular weights [14]. Lately, there has been an increasing attention to utilize the usage of these polymers for biomedical applications because they can be non-toxic, biocompatible, biodegradable, and they can also have a good pharmacokinetics [10,15].

The use of ELPs as drug delivery carriers exploits the properties mentioned above plus the structures they form above their thermal phase transition. The feasibility of loading and entrapping drugs into ELPs offers the potential to deliver drugs to a target tissue by applying external hyperthermia. A study by Adam and co-workers had demonstrated the usage of ELPs in local antibiotics delivery of cefazolin and vancomycin [16]. Other research has been focusing on targeting cancer medicine to tumors utilizing ELPs as drug carriers. Since the tumor has a reduced pH, as low as 6.3 for cells with carcinoma and 6.8 for cells with melanoma, in comparison to the pH level in healthy tissues, the sensitivity of the ELPs to pH level can play a significant role in the treatment of such cells [17,18].

The injection of ELPs for the delivery of drugs to joint spaces and perineural cavities has been studied [10,19-20]. ELPs being investigated as injectable tissue-engineered biomaterials for cartilage repair need to exhibit a transition temperature



around the body temperature, 37°C. The thermally induced aggregated phase of the ELP allows encapsulating of chondrocytes and stem cells and promotes the biosynthesis of cartilage [21].

In addition to their suitability in pharmaceuticals and biomedical applications, ELPs have been emerging as biosensors because of their electrical and optical properties [22]. Their properties can be modified to be able to handle signal detection and signal transmission to electrodes. For example, a phase change of the polymer can produce mechanical work such as closing a valve. ELP and protein-based polymer research are leading to advancements in medicine, technology, and many other fields.

## 1.2 ELP Temperature Dependence

ELPs undergo a reversible phase transition referred to as the inverse temperature transition or lower critical solution temperature (LCST) (Figure 1.2) [23].

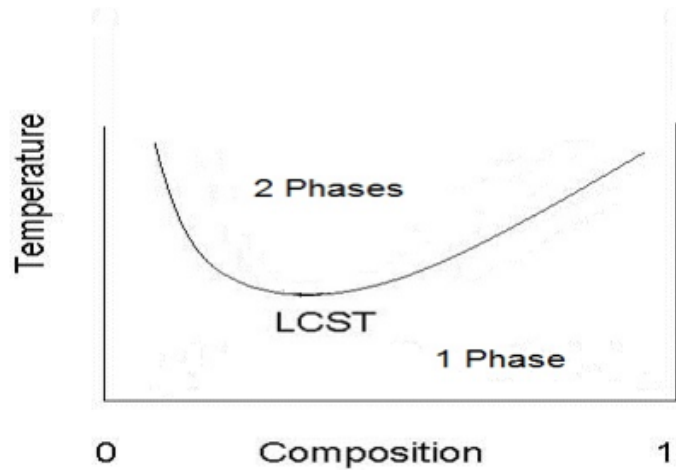


**Figure 1.2: A schematic for the behavior of a polymeric solution that exhibit a lower critical solution temperature (LCST)**

ELPs are soluble in solution below their transition temperature ( $T_t$ ) and they hydrophobically collapse and aggregate above their  $T_t$ , which can be observed as a cloudy

suspension. The transition phase can be determined by measuring the turbidity profile versus temperature. When the temperature of ELP solution increases, the aggregates form a denser viscoelastic phase known as coacervate, a compact form of the ELP that is held together by the hydrophobic forces.

The composition of the poly(GVGVP)–water system versus temperature was studied by Urry et al. [23].

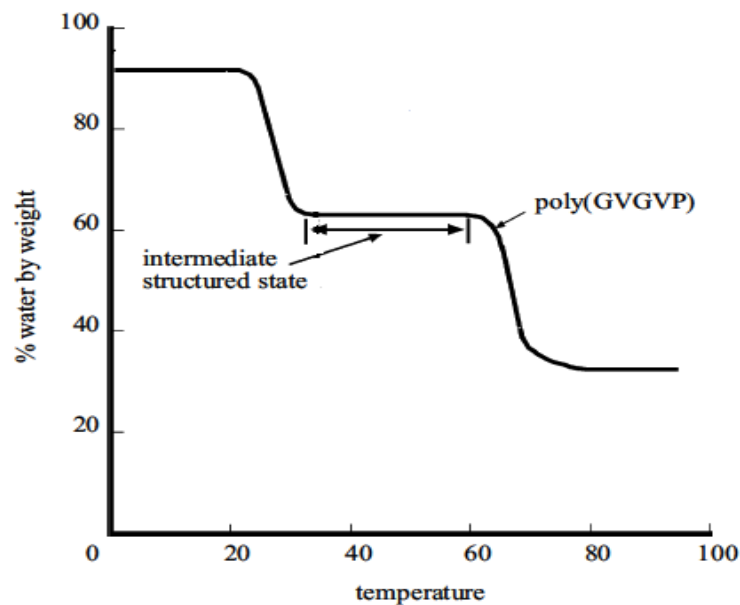


**Figure 1.3: percentage water by weight as a function of temperature for poly(GVGVP)** (Reprinted with permission from Urry, D. W, Hugel T, Seitz M, Gaub H. E, Sheiba L, Dea J, Xu J, and Parker T. "Elastin: a representative ideal protein elastomer." *Philosophical Transactions: Biological Sciences* 357.1418 (2002), 169-184. Royal Society 2011)

Figure 1.3 shows that the ELP is miscible in water and it contains 90% water by weight around 0°C. When the temperature is in between 20 to 30°C, a reversible phase transition is formed with 63 % water by weight. The water composition of this intermediate state is unchanged until the temperature is increased above 60°C. When the temperature is raised

from 60 to 80°C, a slow irreversible transition takes place reducing the water content to 32% by weight. Although keeping the temperature above 80°C for a prolonged time did not result in chain breakage, it resulted in small loss of the polymer, around 1%. Poly(GVGVP) holds a fixed amount of water at the intermediate state and if the temperature is high enough, an irreversible denaturation takes place. Exposure to extreme pH can cause peptide hydrolysis while prolonged exposure to high temperatures causes minimal alteration of the phase transition properties [24]. Precautions are required during chemical synthesis of ELPs to limit the chances of altering the polymer properties. That is not an issue when ELPs are synthesized using DNA technology.

### 1.3 Factors Impacting the Transition Temperature ( $T_t$ )

The transition temperature for a given ELP is highly reproducible and it is dependant on the salt concentration in the solution, the pH of the solvent, the chain length, and the peptide concentration and many other factors such as the sequence of the ELP. When the solution is cooled, the transition is easily reversed.

#### 1.3.1 Salt Concentration

Many researchers have studied the impact of the salt concentrations on the  $T_t$  for ELPs and showed the simplicity of controlling the  $T_t$  by changing the salt concentration [25-29]. Temperature modulated differential scanning calorimetry (TMDSC) has been used to investigate the effect of sodium chloride concentration on the endothermic and the exothermic parts of the  $T_t$  for (GVGVP)<sub>251</sub> [25]. When NaCl is added,  $T_t$  decreases linearly while the change in enthalpy increases (Figure 1.4).

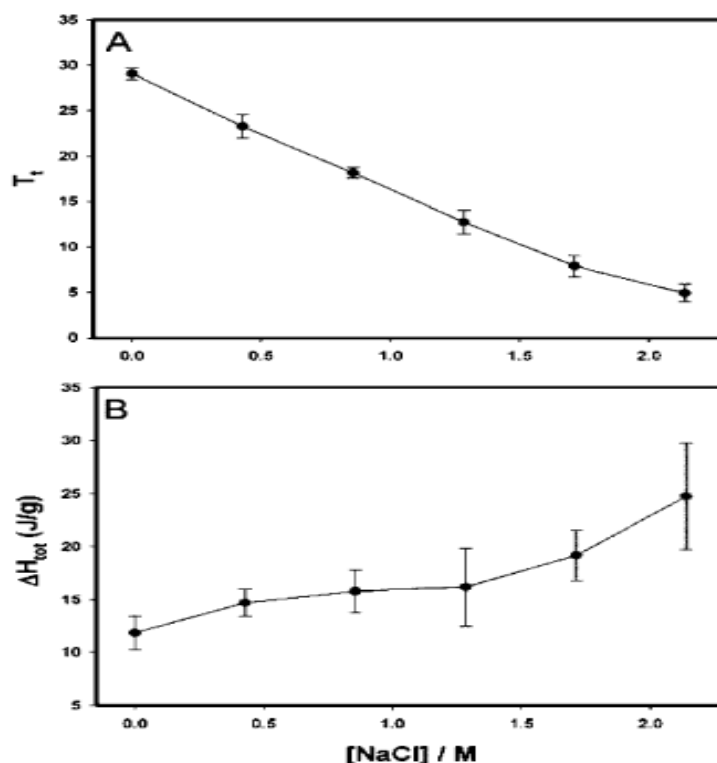


**Figure 1.4: Influence of the salt concentration on the  $T_t$  (A) and enthalpy (B) for a 50 mg/mL (GVGVP)<sub>251</sub> aqueous solution** (Reprinted with permission from Reguera, Javier, Urry, Dan W., Parker, Timothy M., McPherson, David T., and Carlos Rodríguez-Cabello. "Effect of NaCl on the Exothermic and Endothermic Components of the Inverse Temperature Transition of a Model Elastin-like Polymer." *Biomacromolecules* 8.2 (2007), 354-358. ACS 2011)

In this research, the linear dependence of the  $T_t$  on NaCl concentration seems to slightly deviate at higher concentration as seen at the high end of the plot in Figure 1.4 (A). In addition, as the concentration of NaCl is increased, both endothermic and exothermic component are increased. While the exothermic component is associated with the folding, the endothermic behavior is associated with the disruption of the water structure during the temperature induced phase transition. In a conventional DSC, the  $T_t$  as a function of a specific salt concentration can be identified by the minima of the peaks of temperatures versus the endotherm [23]. Other researchers have also shown the linearity function of  $T_t$  for different ranges of concentrations [26, 29]. Ghoorchian et al. found the linearity of  $T_t$  as a function of NaCl concentration for (GVGVP)<sub>40</sub>, (GVGVP)<sub>40</sub>-foldon, and (GVGVP)<sub>120</sub> (Figure 1.5) [29].

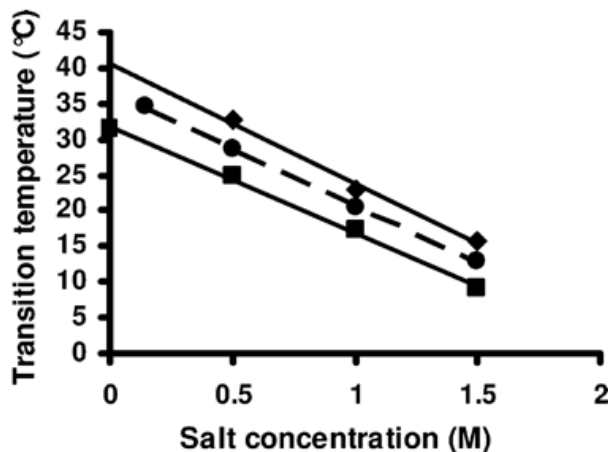


**Figure 1.5:** Effect of salt on the transition temperature of (GVGVP)<sub>40</sub> (diamonds), (GVGVP)<sub>40</sub>-foldon (circles), and (GVGVP)<sub>120</sub> (squares) (Reprinted with permission from Ghoorchian, Ali, James T. Cole, and Nolan B. Holland. "Thermoreversible Micelle Formation Using a Three-Armed Star Elastin-like Polypeptide." *Macromolecules* 43.9 (2010), 4340-4345. ACS 2011)

The presence of the oligomerization domain did not change the linearity function. The slope for the (GVGVP)<sub>40</sub>-foldon and (GVGVP)<sub>120</sub> are the same with higher temperature values for the construct with the foldon. If the amount of salt is increased, the ionic strength of the solution increases leading to an increase in the polarity difference between water molecules and the hydrophobic components and therefore the ELP precipitate at lower temperatures [30].

Another study involved the investigation of the effect of 11 sodium salts, NaSCN, NaI, NaBr, NaNO<sub>3</sub>, NaClO<sub>4</sub>, NaCl, NaF, NaH<sub>2</sub>PO<sub>4</sub>, Na<sub>2</sub>S<sub>2</sub>O<sub>3</sub>, Na<sub>2</sub>SO<sub>4</sub> and Na<sub>2</sub>CO<sub>3</sub>, on two ELP constructs [28]. The two constructs consist of (VPGXG)<sub>120</sub> where the first construct has V at all X residue positions and the second construct has a mixture of V, A, and G at the guest residue position in a 5:2:3 ratio. It was found that the polarization of the interfacial water caused by the addition of kosmotropic anions decreased the  $T_i$  and addition of chaotropic anions also decreased the  $T_i$  but through the surface tension effects. The kosmotropic ions contribute to a better precipitation of the ELPs than the chaotropic ions because of their interactions with the amino acids side chains and the bulk water molecules [31]. Fong et al. also investigated a range of kosmotropic and chaotropic anions in addition

to some cations. He found that the different cations did not have significant effect on the ELP precipitation and  $K^+$ ,  $NH_4^+$ , and  $Na^+$  precipitated the ELP. The anions had more effect on the ELP than the cations and at a low concentration, phosphate and sulfate anions are more effective than chloride [30].

### 1.3.2 The pH Level

The pH at which the phase separation occurs ( $pH_t$ ) is dependent on the ELPs composition, molecular weight, temperature, and concentration. MacKay et al. designed a model that can describe the effect that side chain ionization has on the  $T_t$  [32]. The constructs that were used in the study are acidic ELPs with the sequence of MSKGPG(XGVPG)<sub>40,80,160</sub>WPC. The guest X is a mixture of V, I, and E at 1:3:1 ratio. In addition, basic ELPs with the sequence of MSKGPG(XGVPG)<sub>40,60,100,120</sub>WP and the guest X consisting of a mixture of V, H, G, and A at 1:2:1:1 ratio were also investigated. The acidic ELPs are charged above their  $pK_a$  and they have high  $T_t$ . When their pH is below their  $pK_a$ , the acidic residues become protonated and neutral leading to a decrease in their  $T_t$  (Figure 1.6). On the other hand, the basic ELPs at low pH are soluble and when their pH increases above their  $pK_a$ , they neutralize leading to a decrease in their  $T_t$ .

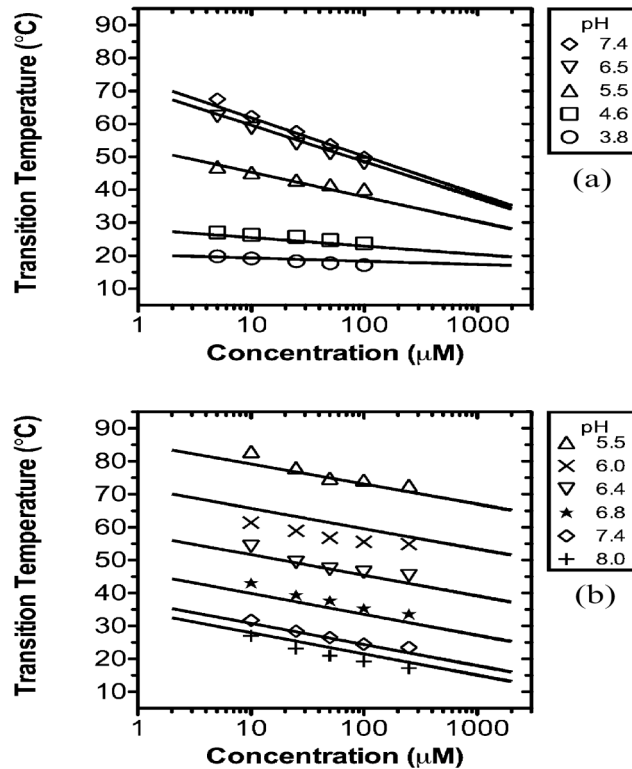


**Figure 1.6: pH and concentration dependence of ELP phase behavior.** ELP transition temperatures are plotted as a function of the logarithm of the polymer concentration. (a) Acidic ELP of 160 pentamers containing guest residues of V/I/E at 1:3:1 ratio with a pKa of 5.29. (b) Basic ELP of 120 pentamers containing guest residues V/H/G/A at 1:2:1:1 ratio with a pKa of 6.22 (Reprinted with permission from MacKay, J. Andrew, Callahan, Daniel J., FitzGerald, Kelly N., and Ashutosh Chilkoti. "Quantitative Model of the Phase Behavior of Recombinant pH-Responsive Elastin-Like Polypeptides." *Biomacromolecules* 11.11 (2010), 2873-2879. ACS 2011)

A model was developed to interpolate between  $T_t$  for fully protonated and fully deprotonated ELPs as a function of pH, equation 1.1.

$$T_t = T_{\text{pro}} + \frac{T_{\text{depro}} - T_{\text{pro}}}{1 + 10^{(\text{p}K_a - \text{pH})}} \quad (1.1)$$

The equation above was used to reach a targeted model that facilitates the calculation of the transition phase pH for an ELP with a specific length and concentration (equation 1.2).

$$\text{pH}_t = \text{pK}_a + \log \left[ \frac{T - T_{c,\text{pro}} - \frac{k_{\text{pro}}}{L} \ln \left[ \frac{C_c}{C} \right]}{T_{c,\text{depro}} - T + \frac{k_{\text{depro}}}{L} \ln \left[ \frac{C_c}{C} \right]} \right] \quad (1.2)$$

Since the ELPs are biologically synthesized, the control over the chain lengths and the concentrations is not a hard task.

### 1.3.3 Chain Length and Concentration

Chilkoti and colleagues had studied the impact that the ELP sequence, chain length, and concentration have on its  $T_t$  [33]. Three ELP libraries of  $(\text{VPGXG})_n$  were used where X is the guest residue with  $\text{V}_1\text{A}_8\text{G}_7$  ratio for the first library,  $\text{V}_5\text{A}_2\text{G}_3$  ratio for the second library, and  $\text{V}_5$  for the third library. The first library is the most hydrophobic leading to the highest  $T_t$  and the third ELP library is the least hydrophobic leading to the lowest  $T_t$  and the second is intermediate between the other two. The  $T_t$  decreases as the concentration of ELPs in each library increases (Figure 1.7).

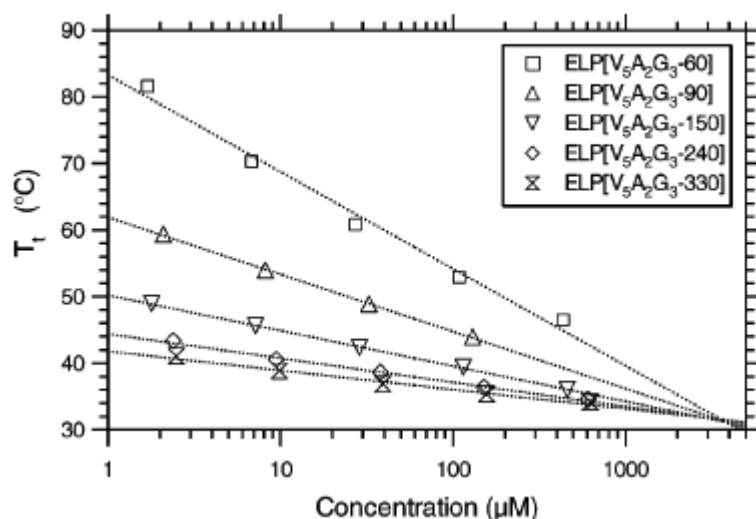


**Figure 1.7:  $T_t$  as a function of concentration for ELP( $\text{V}_5\text{A}_2\text{G}_3$ ) constructs of different chain lengths** (Reprinted with permission from Meyer, Dan E. and Ashutosh Chilkoti. "Quantification of the Effects of Chain Length and Concentration on the Thermal Behavior of Elastin-like Polypeptides." *Biomacromolecules* 5.3 (2004), 846-851. ACS 2011)



The long chains showed a relative constant  $T_t$  while the  $T_t$  increases significantly as the chain length decreases (Figure 1.8).

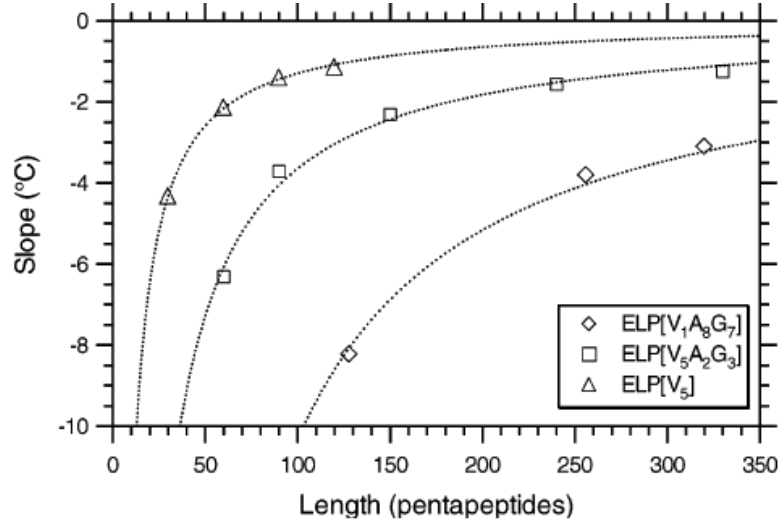


**Figure 1.8: Slope of the linear fits of  $T_t$  versus  $\ln(c)$  as a function of ELP chain length for the three ELP libraries** (Reprinted with permission from Meyer, Dan E. and Ashutosh Chilkoti. "Quantification of the Effects of Chain Length and Concentration on the Thermal Behavior of Elastin-like Polypeptides." *Biomacromolecules* 5.3 (2004), 846-851. ACS 2011)

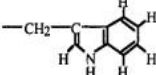
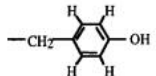
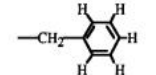
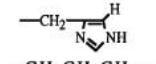
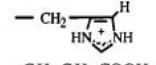
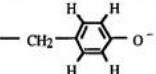
Critical transition temperature,  $T_{t,c}$ , was predicted by a slope approaching zero while critical concentration was predicted by a slope approaching infinity.

MacKay et al. also developed an equation relating the ELP chain length, concentration, and pH to  $T_t$  [32]. A form of the empirical correlation formulated by Meyer and Chilkoti that relates the dependence of  $T_t$  on the concentration and chain length of an ELP library can be substituted into equation 1.1 for both protonated and deprotonated ELP to yield an equation that relates the  $T_t$  to the concentration, length, and pH (equation 1.3).

$$T_t = T_{c,pro} + \frac{k_{pro}}{L} \ln \left[ \frac{C_{c,pro}}{C} \right] + \frac{T_{c,depro} - T_{c,pro} + \frac{1}{L} (k_{depro} \ln \left[ \frac{C_{c,depro}}{C} \right] - k_{pro} \ln \left[ \frac{C_{c,pro}}{C} \right])}{1 + 10^{(pK_a - pH)}} \quad (1.3)$$

where  $C_{c,depro}$ ,  $C_{c,pro}$ ,  $T_{c,depro}$ ,  $T_{c,pro}$ ,  $k_{depro}$  and  $k_{pro}$  are the critical concentration for the deprotonated and for the protonated polymers, the critical  $T_i$  for the deprotonated and for the protonated polymers, and the parameters for the length-concentration interaction for the deprotonated and protonated polymers, respectively. The type of the residue in the ELP sequence can have a significant impact on the transition temperature (Table 1.3).

**Table 1.3: The effects of guest residue composition on the  $T_i$  of ELP homopolymers** (Reprinted with permission from Urry, Dan W. "Physical Chemistry of Biological Free Energy Transduction As Demonstrated by Elastic Protein-Based Polymers." *Journal of Physical Chemistry B* 101.51 (1997), 11007-11028. ASC 2011)

Residue	R Group	Abbreviation	Letter	$T_i^a$	$\Delta H_i$ kcal/mol <sup>d</sup> $\pm 0.05$	$\Delta S_i$ kcal/mol <sup>d</sup> $\pm 0.05$
Tryptophan		Trp	W	-90°C	2.10	7.37
Tyrosine		Tyr	Y	-55°C	1.87	6.32
Phenylalanine		Phe	F	-30°C	1.93	6.61
Histidine		His	H	-10°C		
Proline (calc.) <sup>b</sup>	$-\text{CH}_2\text{CH}_2\text{CH}_2-$	Pro	P	(-8°C)		
Leucine	$-\text{CH}_2\text{CH}(\text{CH}_3)_2$	Leu	L	5°C	1.51	5.03
Isoleucine	$-\text{CH}(\text{CH}_3)\text{CH}_2\text{CH}_3$	Ile	I	10°C	1.43	4.60
Methionine	$-\text{CH}_2\text{CH}_2\text{SCH}_3$	Met	M	20°C	1.00	3.29
Valine	$-\text{CH}(\text{CH}_3)_2$	Val	V	24°C	1.20	3.90
Histidine		His <sup>+</sup>	H <sup>+</sup>	30°C		
Glutamic Acid	$-\text{CH}_2\text{CH}_2\text{COOH}$	Glu	E	30°C	0.96	3.14
Cysteine	$-\text{CH}_2\text{SH}$	Cys	C	30°C		
Lysine	$-\text{CH}_2\text{CH}_2\text{CH}_2\text{CH}_2\text{NH}_2$	Lys <sup>0</sup>	K <sup>0</sup>	35°C	0.71	2.26
Proline (exptl) <sup>c</sup>	$-\text{CH}_2\text{CH}_2\text{CH}_2-$	Pro	P	40°C	0.92	2.98
Alanine	$-\text{CH}_3$	Ala	A	45°C	0.85	2.64
Aspartic Acid	$-\text{CH}_2\text{COOH}$	Asp	D	45°C	0.78	2.57
Threonine	$-\text{CH}(\text{OH})\text{CH}_3$	Thr	T	50°C	0.82	2.60
Asparagine	$-\text{CH}_2\text{CONH}_2$	Asn	N	50°C	0.71	2.29
Serine	$-\text{CH}_2\text{OH}$	Ser	S	50°C	0.59	1.86
Glycine	$-\text{H}$	Gly	G	55°C	0.70	2.25
Arginine	$-\text{CH}_2\text{CH}_2\text{CH}_2\text{NHC}(\text{NH})\text{NH}_2$	Arg	R	60°C		
Glutamine	$-\text{CH}_2\text{CH}_2\text{CONH}_2$	Gln	Q	60°C	0.55	1.76
Lysine	$-\text{CH}_2\text{CH}_2\text{CH}_2\text{CH}_2\text{NH}_3^+$	Lys	K	120°C		
Tyrosinate		Tyr <sup>-</sup>	Y <sup>-</sup>	120°C	0.31	0.94
Aspartate	$-\text{CH}_2\text{COO}^-$	Asp <sup>-</sup>	D <sup>-</sup>	120°C		
Glutamate	$-\text{CH}_2\text{CH}_2\text{COO}^-$	Glu <sup>-</sup>	E <sup>-</sup>	250°C		

Urry and colleagues have studied the impact of different ELP sequences on  $T_i$ . They observed the dependency of  $T_i$  on the hydrophobicity of the guest residue and they quantified the hydrophobicity of the amino acids (Table 1.3) [2].

#### 1.4 Structural Changes of ELPs

In the late 1980's, the research on protein folding intermediates increased rapidly, while earlier studies focused on proving the existence of structural intermediates [34]. Later, conformational changes preceding the phase transition in ELPs have been proven experimentally and computationally [35-38]. The amino acid sequence, the  $\beta$ -secondary structure, and the aggregate structure of the ELP establish the basis of its functionality. Urry's proposed conformation for the relaxed elastomeric state for ELPs, which is demonstrated by the  $\beta$ -spiral structure, is considered as a model for ELPs as shown in Figure 3.4 in Section 3.2 [35,36]. Urry et al. also explained the entropic elastomeric force of polypeptides as a result of internal chain dynamics instead of networks of random chains with a random distribution of end-to-end chain lengths. A study by Brovchenko et al. verified the  $\beta$ -structure through computer simulations on GVG(VPGVG)<sub>3</sub> in the temperature interval between 7°C and 167°C. A rigid conformational state was dominating at low temperatures while a flexible one was dominating at high temperatures [39].

ELPs show a typical elastin-like conformational behavior. When the temperature of an ELP is increased, it shows a decrease in random coil and an increase in  $\beta$ -turn character. An increase in the ELPs order both intermolecularly and intramolecularly result by an increase in temperature [35]. Darwin and colleagues have simulated the  $T_i$  of

elastin using a molecular dynamics program and Urry's  $\beta$ -spiral model. The study supports the critical role of water in determining the elastin's conformational behavior and consequently its inverse temperature transition [40]. Hydration plays a critical role in maintaining proteins functionality and structure and therefore maintaining biological activity. During the initial stage of ELP dehydration, a fibril form by the  $\beta$ -spirals hydrophilic association grows to particles of several hundred nanometers before settling into the phase separated state [23]. In Brovchenko et al. study, the effect of water on the phase reversibility was observed by studying poly( $G_1V_1G_2V_2P$ ). The presence of the methyl group in the residue between P and  $V_1$  of the measured construct had a significant impact on the reversibility of the  $T_i$ . When cooling was applied, the reversibility of poly( $G_1V_1G_2V_2P$ ) suspension containing water molecules between the amide groups was easy. Water molecules remained between the polymer chains at  $T_i$  enabling solubilization during cooling. An expulsion of water from the coacervate is a result of high temperatures, above the  $T_i$ , and at even higher temperatures denaturation of a water containing structure occurs. The denaturation can be reversible by lowering the temperature below  $T_i$ . The poly(GVGVP) had three transitional states where the first state is below the  $T_i$  and the ELP is hydrated and expanded. The second state is above the  $T_i$  where the ELP is more compact and aggregated. The final state is significantly above the  $T_i$  where denaturation takes place [39].

The effect of  $\gamma$ -irradiation on the hydrodynamic radius of the polymer in solution was studied by Jonghwilee et al. [41]. Equilibrium swelling ratios of repeated pentapeptide sequences after slight cross-linking by  $\gamma$ -irradiation were investigated above and below their  $T_i$ . The dose of the  $\gamma$ -irradiation had an impact on the equilibrium

swelling ratio and it decreased as the  $\gamma$ -irradiation increased indicating the decrease of molecular weight between the cross-links (Figure 1.9). On the contrary,  $\gamma$ -irradiation dose had no effect on the swelling ratio of the polymer above its  $T_i$ .

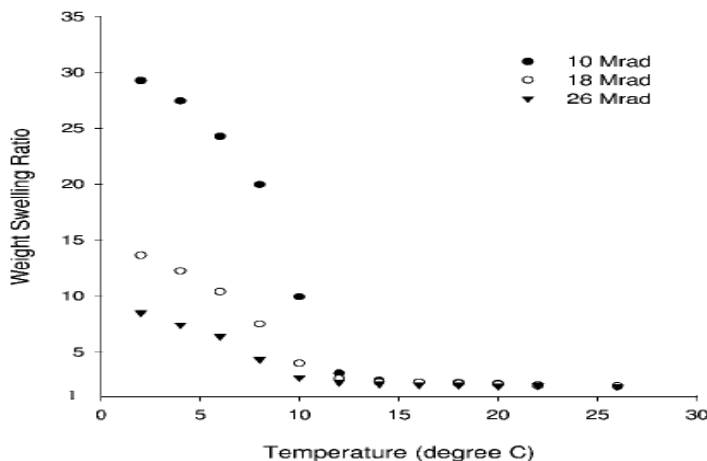


**Figure 1.9: Equilibrium weight swelling ratio of pentapeptides in water as a function of temperature and  $\gamma$ -irradiation dose** (Reprinted with permission from Lee, Jonghwi, Christopher MacOsco, and Dan Urry. "Phase transition and elasticity of protein-based hydrogels." *Journal of Biomaterials Science, Polymer Edition* 12.2 (2001), 229-242. ACS 2011)

In this project, an oligomerization domain, a foldon, is present. Oligomeric-coiled coil motifs can be found in many proteins such as in fibrin promoting the assembly of tail fibers and also working as a sensing device [42]. It has a structure of triple coiled coil helices. In addition to fixing multiple polymeric chains in one region, the oligomerization domain can have an impact on the polymeric chains properties [43]. Ghoorchian et al. showed the effect that foldon has on the transition temperature of the ELP (Figure 1.10) [29]. Even though (GVGVP)<sub>40</sub>-foldon and (GVGVP)<sub>120</sub> have similar molecular weights, the  $T_i$  for (GVGVP)<sub>40</sub>-foldon is higher because of the foldon presence.

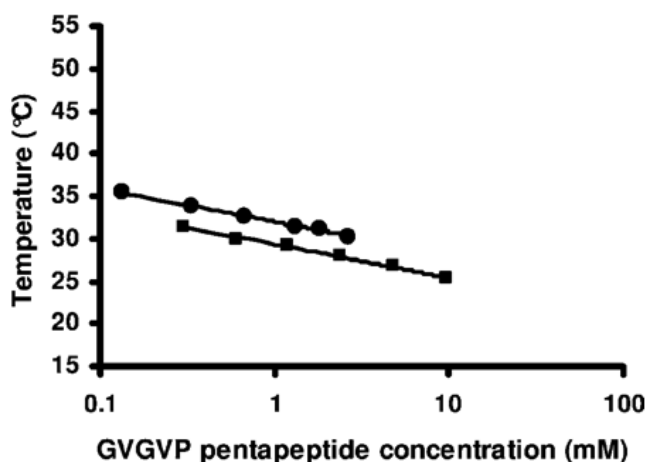


**Figure 1.10:** Transition temperatures of (GVGVP)<sub>40</sub>-foldon (circles) and (GVGVP)<sub>120</sub> (squares) as a function of molar concentration of GVGVP pentapeptides (Reprinted with permission from Ghoorchian, Ali, James T. Cole, and Nolan B. Holland. "Thermoreversible Micelle Formation Using a Three-Armed Star Elastin-like Polypeptide." *Macromolecules* 43.9 (2010), 4340-4345. ACS 2011)

## 1.5 Characterization of ELPs

Variable techniques and methods have been developed over the years to characterize the solution properties of ELPs. The vast varieties of the characterization techniques to characterize proteins are useful for characterizing biophysical, structural, and rheological properties of ELPs. The following sections will briefly discuss the methods to characterize the previously mentioned properties. Later, more focuses will be shifted on the scope of the paper of characterizing ELPs conformational changes using capillary viscometry.

### 1.5.1 Biophysical Properties Characterization

ELPs concentration can be determined using spectroscopy while the molecular weight can be measured by sodium dodecyl sulfate polyacrylamide gel electrophoresis (SDS-PAGE) and mass spectrometry methods such as matrix-assisted laser desorption ionization (MALDI-MS). The lower critical solution temperature (LCST) can be

determined by turbidity measurement, usually with optical density of 350 nm [44,45]. The binding behavior of ELPs can be determined using surface plasmon resonance spectroscopy (SPR).

### 1.5.2 Structural Properties Characterization

The structural properties of ELPs such as hydrodynamic radius and folding are significant to their applications. The structural information of ELPs can be determined using nuclear magnetic resonance (NMR) and X-ray [46-48]. The folding of the ELP can be investigated using circular dichroism (CD) or differential scanning microcalorimetry (DSC) [49,50,29]. The hydrodynamic radius can be determined using dynamic light scattering (DLS) which is very helpful in the investigation of the formation of the self assembled particles, micelles [51,29]. This paper will fill the gap for the observation of the structural changes and the hydrodynamic radius changes using capillary viscometry as it will be discussed later.

### 1.5.3 Bulk Properties Characterization

Relationship between different moduli such as the elastic, the viscous, and the dynamic shear modulus as function of temperature, time, strain, and other parameters can produce measurements that will lead to a relationship between the ELP bulk properties and its molecular structure. The swelling of the ELPs can be characterized by the swelling ratio (Figure 1.9). A swelling ratio with value greater than unity points to the swelling of the ELPs and the value of less than unity points to the contraction of the ELPs.

## 1.6 Polymer Characterization Using Capillary Viscometer

### 1.6.1 Viscosity

Viscometry is one of the most common and basic applications to examine the structure and the properties of a polymeric solution. Viscosity is a measure of the resistance of fluid to flow (Figure 1.11) [51]. The fluid is deformed when flowing into the capillary by shear stress or tensile stress.

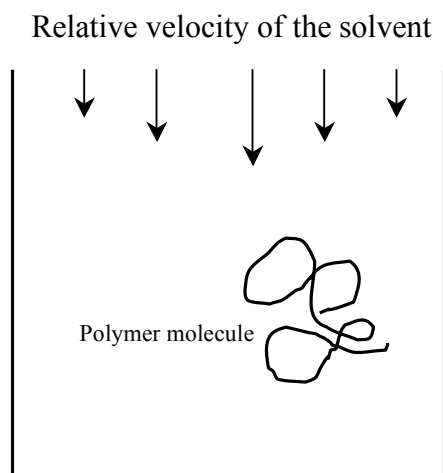


**Figure 1.11: The effect of shear rate on the polymer chain rotation** (Adapted from reference [51])

If a dilute polymeric solution is flowing through a capillary, it will experience the different shear rates on its different parts as it rotates down the capillary (Figure 1.11). As a result, an increase in the frictional drag will take a place yielding an increase in the viscosity [51].

A Cannon-Ubbelohde Semi-Micro viscometer is used in this project to measure the viscosity of the polymer fluids. The instrument has the advantage of obtaining values that are independent of the concentration. It also uses a capillary-based method of



measuring the relative viscosity by applying Hagen–Poiseuille law, equation 1.4. The law gives the pressure drop in a fluid flowing through a cylindrical pipe [52].

$$\eta = \pi R^4 P / 8QL \quad (1.4)$$

There are assumptions that are built in this equation where the flow is laminar and incompressible. The flow also goes through a constant circular cross-section, capillary, that is longer than its diameter. The letter  $R$  stands for the radius of the capillary,  $P$  is the hydrostatic pressure,  $Q$  is the volumetric flow rate, and  $L$  is the length of the capillary. The dynamic viscosity,  $\eta$ , can have the unit of Pa·s. Since the volume of the bulb in the Ubbelohde viscometer is constant, the flow rate is inversely proportional to the traveling time of the fluid between the two marks on the viscometer. Taking into an account the proportionality of the hydrostatic pressure to the density will lead to one of the most fundamental relations of capillary viscosity, equation 1.5.

$$\eta \propto t \rho \quad (1.5)$$

The relation in 1.5 can be specific for the pure solvent or the polymeric solution.

$$t_{\text{solvent}} \propto \eta_{\text{solvent}} / \rho_{\text{solvent}} \quad (1.6)$$

$$t_{\text{solution}} \propto \eta_{\text{solution}} / \rho_{\text{solution}} \quad (1.7)$$

A relative viscosity of the solution to that of the solvent can be defined as presented in equation 1.8.

$$\eta_{\text{relative}} = \eta_{\text{solution}} / \eta_{\text{solvent}} \quad (1.8)$$

Since the polymeric solutions that are used in this project are dilute, the ratio of the solution to solvent densities can be taken as unity and the relative viscosity can be measured by measuring the elution time of the solution over the elution time of the pure solvent. Since the relative viscosity is always larger than unity, another dimensional

viscosity called specific viscosity is introduced by subtracting one from the relative viscosity. The inherent viscosity,  $\ln \eta_{relative}/c$ , and the reduced viscosity,  $\eta_{specific}/c$ , can be plotted against concentrations using Kraemer and Huggins equations, equation 1.19 and equation 1.10 respectively. Then, both terms can be extrapolated to zero concentrations to find the intrinsic viscosity,  $[\eta]$ . Intrinsic viscosity is the ratio of the solution's specific viscosity to the solute's concentration, extrapolated to zero. [51].

$$\eta_{specific}/c = [\eta] + k'[\eta]^2 c \quad (1.9)$$

$$(\ln \eta_{relative})/c = [\eta] - k''[\eta]^2 c \quad (1.10)$$

The values for  $k'$  and  $k''$  for many polymer-solvent systems are 0.35 and 0.15 respectively. If the  $k'$  and  $k''$  do not add up to 0.5, it can indicate molecular aggregation or the existence of other problems in the system.

#### 1.6.2 Mark-Houwink-Sakurada (MHS) Constants and ELPs Conformation

If the molecular weights of the polymers are known, such as the case in this project, and their intrinsic viscosities are calculated according to some experimental measures, Mark-Houwink-Sakurada (MHS) relation in equation 1.11 can be utilized to calculate the  $a$  and  $K$  constants for a specific polymer-solvent system at a specific temperature. In addition, a double logarithm plot of molecular weights versus their intrinsic viscosities at a given temperature can also facilitate the calculation of the MHS constants,  $a$  and  $K$ . The slope will be the constant  $a$  and the intercept will be the logarithm of the constant  $K$  [51].

$$[\eta] = K(M_v)^a \quad (1.11)$$

The exponent  $a$  provides information about the geometry of the polymeric molecules in the solvent (Table 1.4).

**Table 1.4: Values of the Mark-Houwink-Sakurada exponent  $a$  and its different geometrical interpretations** (Adapted from reference [51])

$a$	Physical Interpretation
0	Rigid Spheres
0.5 – 0.8	Random Coils
1.0	Stiff Coils
2.0	Rods

As the temperature increases, the goodness of the solvent decreases leading to an aggregate and a compact form of the polymer. The values of the constants  $a$  and  $K$  are dependent on the choice of the polymer-solvent system and the temperature. Changing any of the previous parameters can produce a change in the polymer conformation and therefore change in the values of the constant  $a$ .

### 1.6.3 Sphere Equivalent Radius of ELPs

Einstein had derived an expression for the viscosity in a dilute solution assuming uniform, rigid, and non-interacting spheres [51].

$$\eta = \eta_{\text{solvent}} (1 + 2.5v_2) \quad (1.12)$$

The parameter  $v_2$  represents the volume fraction of spheres. The dimension of the coiled polymer will be approximated using an equivalent hydrodynamic sphere,  $R_e$  (Figure 1.12) [51].

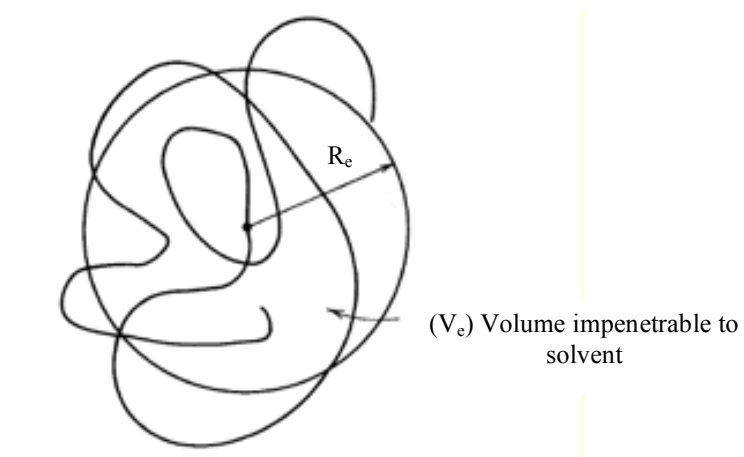


**Figure 1.12: The equivalent sphere model** (Adapted from reference [51])

The molecular weight and the intrinsic viscosity will be related to  $R_e$  later in Section 3.2.

## CHAPTER II

### MATERIALS AND METHOD

#### 2.1 Overview

Three ELP constructs were expressed and purified according to specific laboratory guidelines. After the ELPs were synthesized, their concentrations were measured. In addition, a verification of the viscometer calibration was completed. Then, the viscosity of the solvent and the viscosity of different concentrations of each construct at different temperatures were measured.

#### 2.2 ELPs Expression and Purification

The desired elastin-like polypeptides (ELPs) for this project are presented in Table 2.1. They are expressed and purified according to specific laboratory protocols.

**Table 2.1: The novel ELPs along with their amino acid sequences and their corresponding molecular weights**

ELP	Amino Acid Sequence	Molecular Weight (g/mole)
(GVGVP) <sub>40</sub>	MG(GVGVP) <sub>40</sub>	17063
(GVGVP) <sub>40</sub> -foldon	MG(GVGVP) <sub>40</sub> GWPGYIP EAPRDGQAYVRKDGEWVLLSTFL	20143
(GVGVP) <sub>60</sub> -foldon	MG(GVGVP) <sub>60</sub> GWPGYIP EAPRDGQAYVRKDGEWVLLSTFL	28333

The foldon is the highlighted part of the amino acid sequences in Table 2.1. Since the ELPs were produced using DNA recombinant technology, there was control over their chains lengths and their amino acid sequence. The molecular weights of the monodisperse ELPs in Table 2.1 were calculated from the amino acid compositions.

### 2.2.1 Media Preparation

A mixture of 10 g of peptone, 5 g of sodium chloride, and 5 g of yeast were added to a large flask, a two-liter flask, under the hood in the laboratory. One liter of distilled water was added to the mixture and the flask was sealed with foil, taped with an autoclave tape, and autoclaved. The media was set to cool after autoclaving and after it was cool enough, around room temperature, 0.1 g of ampicillin was mixed with 1 ml of the media. Then, the ampicillin mixture was added to the media inside the flask.

### 2.2.2 Starting the Culture

A 20 ml aliquot of the prepared media was added to a culture tube and a frozen sample culture of bacteria that express the desired construct was added to the tube to initiate growth. Then, the tube was placed into an incubator at 37°C and 300 rpm for over 12 hours but not more than 16 hours. Later, a BioMate 3 UV-Visible Spectrophotometer was zeroed with a clear media from the flask. The spectrophotometer mode was set to cell growth at 600 nm. After the spectrophotometer was zeroed, the 20 ml culture tube was emptied into the media flask inside the incubator. The absorbance was measured every 15 minutes and when it was approaching unity, 0.1 mM of isopropyl- $\beta$ -D-thiogalactopyranoside (IPTG) was added to the flask. The solution was kept in the incubator for more than 4 hours at the same previous setting of 37°C and 300 rpm. After 4 hours, the culture was centrifuged at 10°C and 9000 rpm and the pellet was collected.

### 2.2.3 Sonication

After the cold centrifugation, the pellet was resuspended in phosphate buffered saline and collected in a 50 ml tube. The tube was placed in an ice bath under the tip of the sonication unit, model 550 sonic dismembrator with a tip of 0.5" diameter. After the tip was cleaned with methanol and distilled water and dried with clean paper towel, the sonication was tuned according to the laboratory manual. After that, the nozzle was placed into the 50 ml tube and the sonication unit was started at 10 amps and for 3 minutes to break up the cells inside the tube.

#### 2.2.4 Purification

After sonication, the content of the tube went through multiple cold centrifugations at 10°C and hot centrifugations at 40°C as follow:

Cold → Hot → Cold → Hot → Cold

Since the ELPs are completely soluble at low temperatures, below their  $T_i$ , the liquid fraction was collected after the cold centrifugations. ELPs also aggregate at high temperatures, above their  $T_i$ , and therefore the pellet was collected after hot centrifugations. The centrifugation unit was allowed to cool to room temperature after hot cycles and it was also allowed to warm after cold cycles. After the final cycle of cold centrifugation, the liquid fraction was collected and it was filtered through a Millex GS filter with 0.22  $\mu\text{m}$  pore size.

#### 2.3 Concentration Measurements

The concentrations of the samples were measured using a BioMate 3 UV-Visible Spectrophotometer and 1 cm x 1 cm QS quartz cuvettes at a wavelength of 280 nm. Initially, pure PBS solvent was used as the standard sample to zero the absorbance of the spectrophotometer. When the concentrations of some of the constructs were high or turbid at room temperature, diluted samples for the purpose of measuring the concentrations were used.

#### 2.4 Verifying the Viscometer Calibration.

Calibration of an apparatus is an essential part of many experiments. It is necessary to verify the viscometer constant to obtain accurate viscosity measurements. A



Cannon-Ubbelohde Semi-Micro viscometer size 25 (Cannon Instrument Company) was used in this project (Figure 2.2). The constant of the viscometer (0.001909 cSt/s) can be found in the viscometer certificate of calibration. The constant was verified through measuring the viscosity of water, using the viscometry bath (Figure 2.1), and comparing it to the literature values and it was verified to be 0.001909 cSt/s [53].

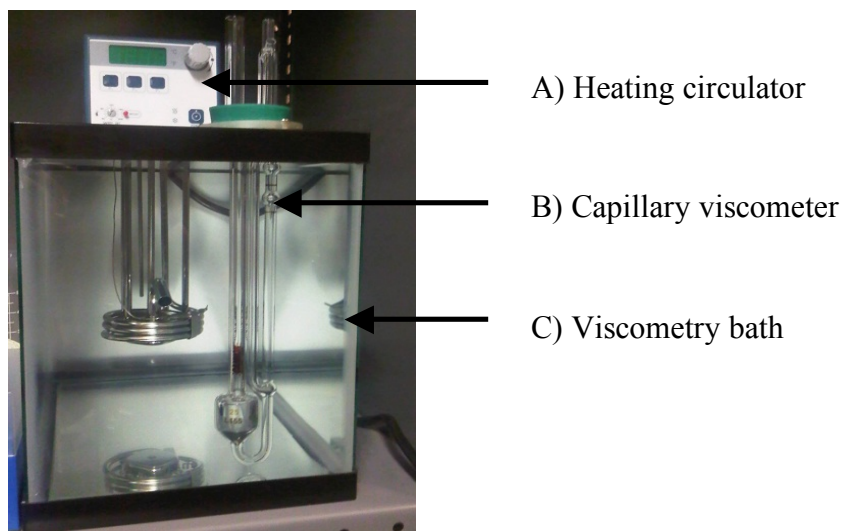


**Figure 2.1: Viscometry bath with a heating circulator**

The viscometry bath is 8" by 13.5" with a height of 10" and is filled with water. The viscometer can be observed through the clear walls of the bath. The bath has a VWR heating circulator (Model 1122S) that has a range of 5°C above the ambient temperature to 200°C with an accuracy of  $\pm 0.1^\circ\text{C}$ . Since the heating circulator will not work below ambient temperature, the viscometry bath was placed into a cold room at 5°C.

The flow time for the water was measured at different temperatures. A known amount of the water was loaded into the Cannon-Ubbelohde Semi-Micro viscometer (Figure 2.2). The heating circulator in the viscometer bath was set to a desired temperature and there was a wait of around 10 minutes to allow the temperature of the

bath to equilibrate (Figure 2.1). Suction was applied at point A in Figure 2.2 to draw the water up the capillaries and above the upper timing line while point B was plugged. When the water passed the upper timing line, the opening of B was unplugged first then the suction was released. The effluent time of the water was measured using a stopwatch and the timing was also verified through video recording. A second measurement for the time was done to assure an agreement between the readings. A third, and in some cases a fourth, measurement was taken when the first two measurements were not consistent. The previous process was repeated for a range of temperatures in between 20°C to 30°C.

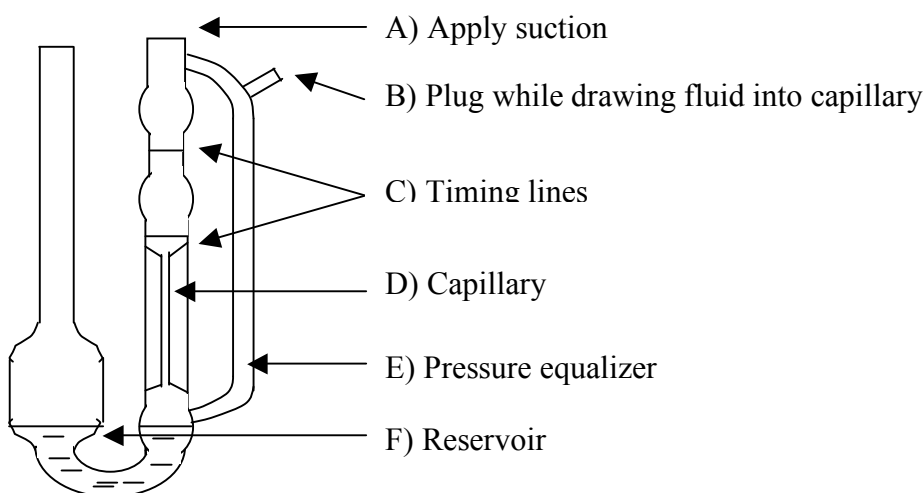


**Figure 2.2: Schematic drawing of the cannon capillary viscometer**

A plot comparing literature and experimental water viscosities is presented in Appendix

A. The correction factor for the viscometer was verified to be  $0.001909 \text{ mm}^2/\text{s}^2 \text{ (cSt/s)}$ .

## 2.5 Viscosity Measurements

After verifying the viscometer constant of 0.001909 cSt/s, the viscometer was used to determine the flow time for the solvent and the ELP constructs of (GVGVP)<sub>40</sub>-foldon,

(GVGVP)<sub>60</sub>-foldon and (GVGVP)<sub>40</sub>. The same procedure that was used to measure the water effluent time was also used to measure the efflux time for the PBS solvent and the ELP constructs. The measurements for the ELPs are taken for a range of temperatures starting at 20°C and stopping where the solution turned turbid as shown in Figure 2.3, where transition temperature is reached.



**Figure 2.3: (a) Clear solution of 448  $\mu$ M of (GVGVP)<sub>40</sub>-Foldon at 25°C. (b) Turbid solution of 448  $\mu$ M of (GVGVP)<sub>40</sub>-foldon at 37°C. The transition temperature for 448 $\mu$ M of (GVGVP)<sub>40</sub>-foldon is at 28°C**

Since the concentration of the sample in the viscometer was known and the experimental measurements on it for different temperatures were completed, dilution of the sample was taken inside the viscometer and verified later using the spectrophotometer.

## CHAPTER III

### RESULTS AND DISCUSSION

#### 3.1 Viscosity Calculations and Analysis

Viscosity measurements were utilized to observe the change in the ELPs conformation. Once the efflux times for PBS and the ELP construct solutions were obtained, a relationship based on Poiseuille's law (Equation 1.4) was used. Later, the viscosity of the solution relative to the viscosity of the solvent, called the relative viscosity, was calculated. Since the solutions used in this project were dilute, the ratio for the density of the solution to the density of the solvent is close to unity and therefore Poiseuille's law reduces to the following form:

$$\eta_{\text{relative}} = \eta_{\text{solution}} / \eta_{\text{solvent}} = t_{\text{solution}} / t_{\text{solvent}} \quad (3.1)$$

Where  $\eta$  is viscosity coefficient and  $t$  is the time that is required for the fluid to pass from one line to the other in the viscometer. The relative viscosity is larger than unity because the time of the solution is in the numerator and the time for the pure solvent is in the denominator. An additional definition of unitless viscosity is measured by the fractional change of the solution to solvent viscosities called the specific viscosity.

$$\eta_{\text{specific}} = (\eta_{\text{solution}} - \eta_{\text{solvent}}) / \eta_{\text{solvent}} = \eta_{\text{relative}} - 1 \quad (3.2)$$

The kinematic viscosities in mm<sup>2</sup>/s (cSt) were obtained by multiplying the efflux time in seconds by the viscometer constant 0.001909 mm<sup>2</sup>/s<sup>2</sup> (cSt/s) (Figure 3.1).

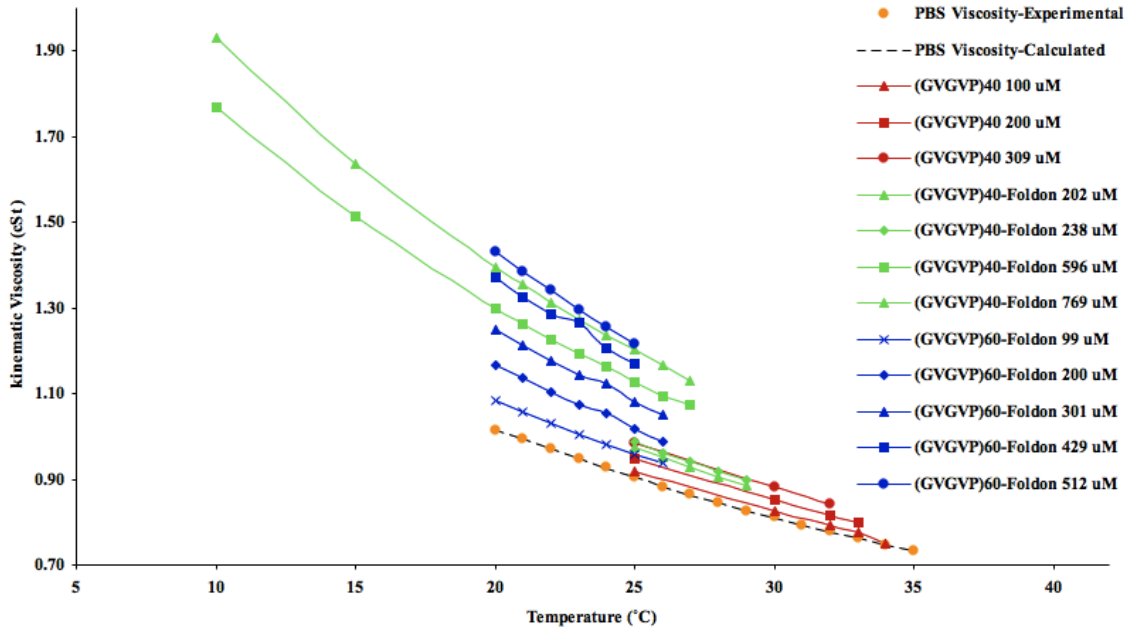


**Figure 3.1: The kinematic viscosity of PBS and different concentrations of (GVGVP)<sub>40</sub>-foldon, (GVGVP)<sub>60</sub>-foldon and (GVGVP)<sub>40</sub>**

The concentration and the temperature effects on the viscosity are evident by Figure 3.1. The viscosity decreases upon an increase in the temperature or a decrease in the concentration. When the temperature increases, more of the solvent diffuses out of the polymer [2]. The polymer becomes more compact and as a result the compact polymer produces less resistance of flow. An equation for the solvent (PBS) efflux time as a function of temperature was formed using data from Figure 3.1.

$$\text{PBS}_{\text{efflux time}} [\text{s}] = -1.19 \times 10^{-4} T^4 + 9.22 \times 10^{-3} T^3 - 1.64 \times 10^{-2} T^2 - 19.87 T + 882.86 \quad (3.3)$$

The relative and the specific viscosities are both dependent on the polymer concentration as described by the Kraemer and Huggins equations, equation 3.4 and 3.5 respectively.

$$\eta_{\text{specific}}/c = [\eta] + k'[\eta]^2 c \quad (3.4)$$

$$(\text{Ln } \eta_{\text{relative}})/c = [\eta] - k''[\eta]^2 c \quad (3.5)$$

Kraemer and Huggins equations are utilized to calculate the intrinsic viscosity  $[\eta]$ .

$$[\eta] = \lim_{c \rightarrow 0} \eta_{\text{specific}}/c \approx \lim_{c \rightarrow 0} (\text{Ln } \eta_{\text{relative}})/c \quad (3.6)$$

Both lines for  $\eta_{\text{specific}}/c$  versus  $c$  and also  $(\text{Ln } \eta_{\text{relative}})/c$  versus  $c$  should give the same intercept,  $[\eta]$ . The intrinsic viscosity,  $[\eta]$ , is the ratio of the solution's specific viscosity to the solute's concentration extrapolated to zero. It is an expression for the polymeric volume per unit mass having units of ml/mg [51]. The sum of  $k'$  and  $k''$  for most polymer-solvent systems in the Kraemer and Huggins equations is 0.5. Figure 3.2 is the product of plotting Kraemer and Huggins equations to estimate the intrinsic viscosity.

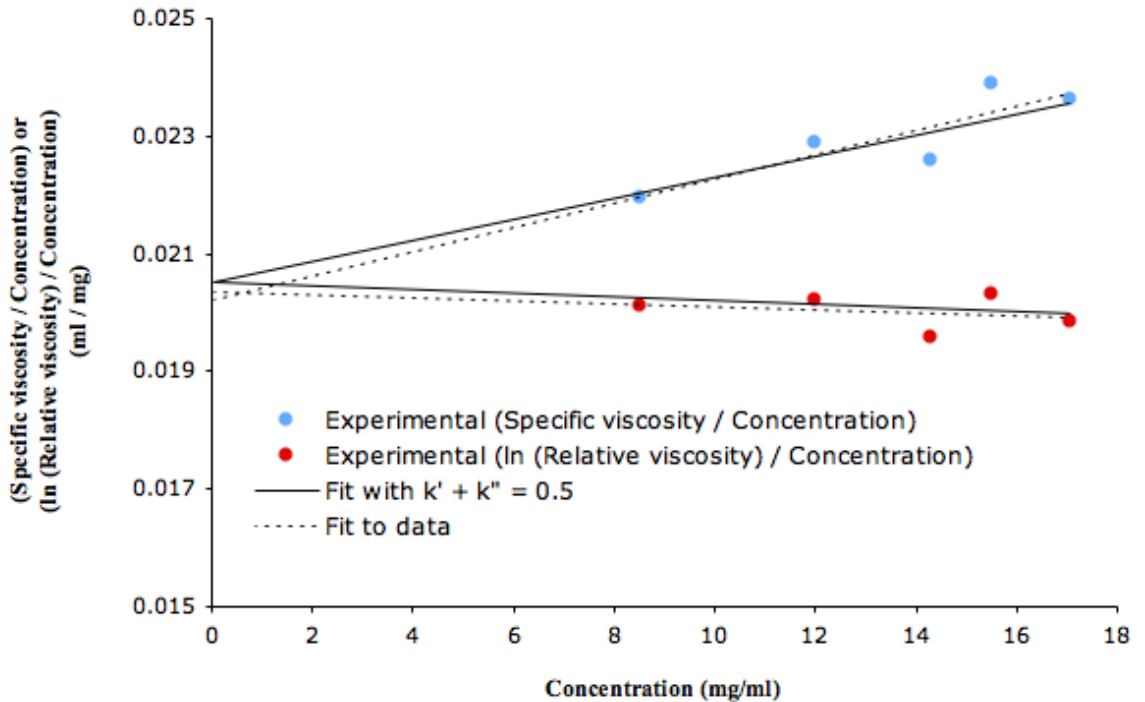


**Figure 3.2: Plot of  $\eta_{\text{specific}}/c$  versus  $c$  and also  $(\text{Ln } \eta_{\text{relative}})/c$  versus  $c$  for (GVGVP)<sub>40</sub>-foldon at 20°C extrapolated to zero concentration to find an intrinsic viscosity of 0.021 ml/mg with a standard deviation  $\pm 3\%$ .**

Data for very low concentrations could not be obtained because of high errors. The specific viscosity is a product of unity subtracted from the relative viscosity. When the concentration is small, the specific viscosity will be closer to zero and therefore it produces a large error. High concentration could not be used because the solution will not be considered dilute. Since the ELPs are small in size and data for very low and very high concentrations could not be obtained, the investigated data clusters close to each other. The clustered data causes the extrapolation to zero concentration to produce large deviations in the values of the intercept. Assuming  $k'$  and  $k''$  add up to 0.5 greatly reduces the errors of extrapolation because it couples the two equations. Fits of the data by minimizing the least sum square of the error were obtained based on assuming  $k'$  and  $k''$  adds up to 0.5. The complete set of figures for intrinsic viscosity data obtained in this project can be found in Appendix B.

The summation value for the  $k'$  and  $k''$  is known and values for the relative viscosity are available through the experimental measurements, as a result, the Kraemer and the Huggins equations can be algebraically added to form an equation for the intrinsic viscosity based on a measurement at a single concentration.

$$[\eta] = [2 (\eta_{\text{specific}} - \ln \eta_{\text{relative}})]^{0.5} / c = [2 ((1 - \eta_{\text{relative}}) - \ln \eta_{\text{relative}})]^{0.5} / c \quad (3.7)$$

Now, the intrinsic viscosity can be determined for viscosity measurements at each concentration using equation 3.7 (Figure 3.3). The intrinsic viscosity of (GVGVP)<sub>40</sub>-foldon and (GVGVP)<sub>60</sub>-foldon in PBS exhibit a linear relationship with temperature.

$$\text{For (GVGVP)}_{40}\text{-foldon:} \quad [\eta] = - 5.11 \times 10^{-4} T + 3.06 \times 10^{-2} \quad (3.8)$$

$$\text{For (GVGVP)}_{60}\text{-foldon:} \quad [\eta] = - 7.04 \times 10^{-4} T + 3.93 \times 10^{-2} \quad (3.9)$$

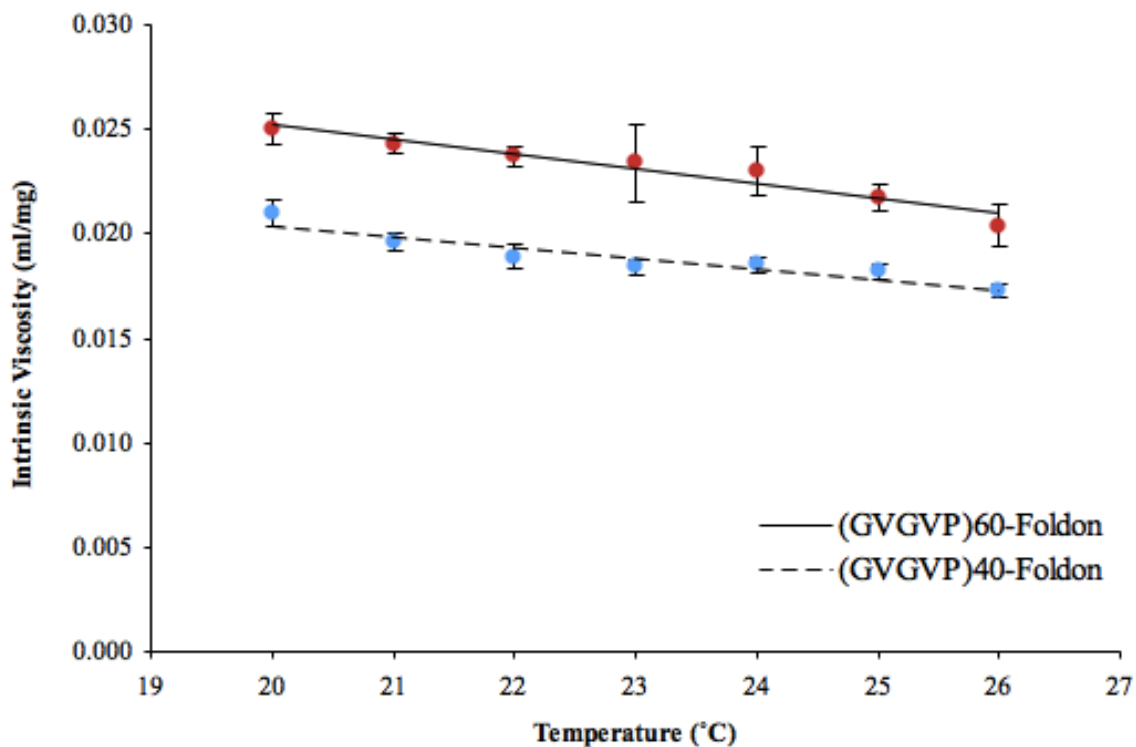


**Figure 3.3: The intrinsic viscosities for (GVGVP)<sub>40</sub>-foldon and (GVGVP)<sub>60</sub>-foldon versus temperature with their standard deviations**

For a random coil polymer, the viscosity is a molecular weight dependent as described by the Mark-Houwink-Sakurada (Equation 1.11). The (GVGVP)<sub>60</sub>-foldon has a larger molecular weight than (GVGVP)<sub>40</sub>-foldon and therefore it has larger viscosity values. From the calculated intrinsic viscosities and known molecular weights for (GVGVP)<sub>40</sub>-foldon and (GVGVP)<sub>60</sub>-foldon, Mark-Houwink-Sakurada constants can be calculated for these novel polypeptides as will be discussed in Section 3.3.

### 3.2 Temperature Dependent ELP Conformational Changes

When the temperature is increased, the conformation of the linear polymers in (GVGVP)<sub>40</sub> changes (Figure 3.4) [2,29,35].



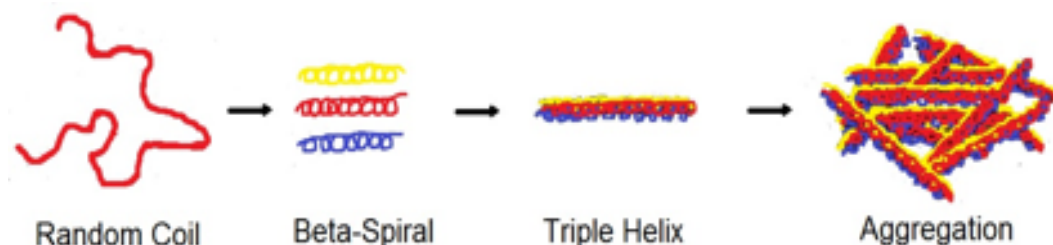


**Figure 3.4: The transition of a random coil polymer as a function of increase in temperature. The final form is an aggregate at the transition temperature of the polymer** (Modified from reference [29])

Once the transition temperature is reached, the helices aggregated and the solution turns cloudy (Figure 2.3). The same effects occur in the three-armed star ELPs, (GVGVP)<sub>40</sub>-foldon and (GVGVP)<sub>60</sub>-foldon, where the goodness of the solvent decreases with the increase in temperature and causes the arms of the polymer to fold together (Figure 3.5) [29].

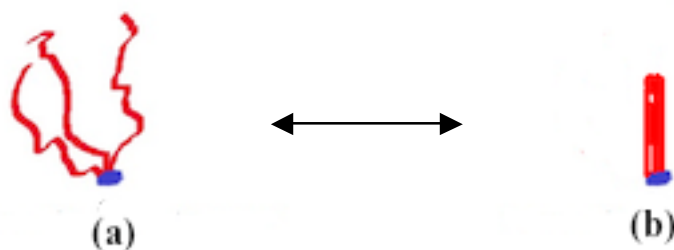


**Figure 3.5: The folding of the three-armed star polymer caused by an increase in temperature** (Modified from reference [29])

The aggregation of (GVGVP)<sub>40</sub>-foldon and (GVGVP)<sub>60</sub>-foldon, the three-armed star ELPs, occur at lower temperature than the linear ELP in (GVGVP)<sub>40</sub>. In the later one the chains have to diffuse to find each other to form an aggregate while in the three-armed star ELPs each three chains are attached by a foldon and therefore aggregation takes place at lower concentrations.

The hydrodynamic equivalent radius of the polymer is another subject that can be investigated using viscometry measurements. Considering Einstein's expression for the

viscosity in a dilute solution for uniform and non-interacting spheres in equation 1.12, the viscosity is dependent on the volumetric fraction of the spheres in the solution. If we consider the polymers being studied acting as spheres, a hydrodynamic equivalent sphere radius ( $R_e$ ) will be a measure of the spheres dimensions and Einstein's expression can be rewritten as [51]:

$$(\eta / \eta_{\text{solvent}}) / \eta_{\text{solvent}} = \eta_{\text{specific}} = 2.5(n/V)V_e \quad (3.10)$$

Where  $n$  is the number of polymers and  $V$  is the total volume of the polymers ( $n V_e$ ) over the total solution volume. The equivalent volume ( $V_e$ ) of an individual polymer can be written as  $(4\pi/3)(R_e)^3$  for a spherical geometry. An increase in the equivalent radius of the polymers will yield an increase in the volumetric fraction of the spheres. That will cause an increase in the intrinsic viscosity (Figure 3.6).

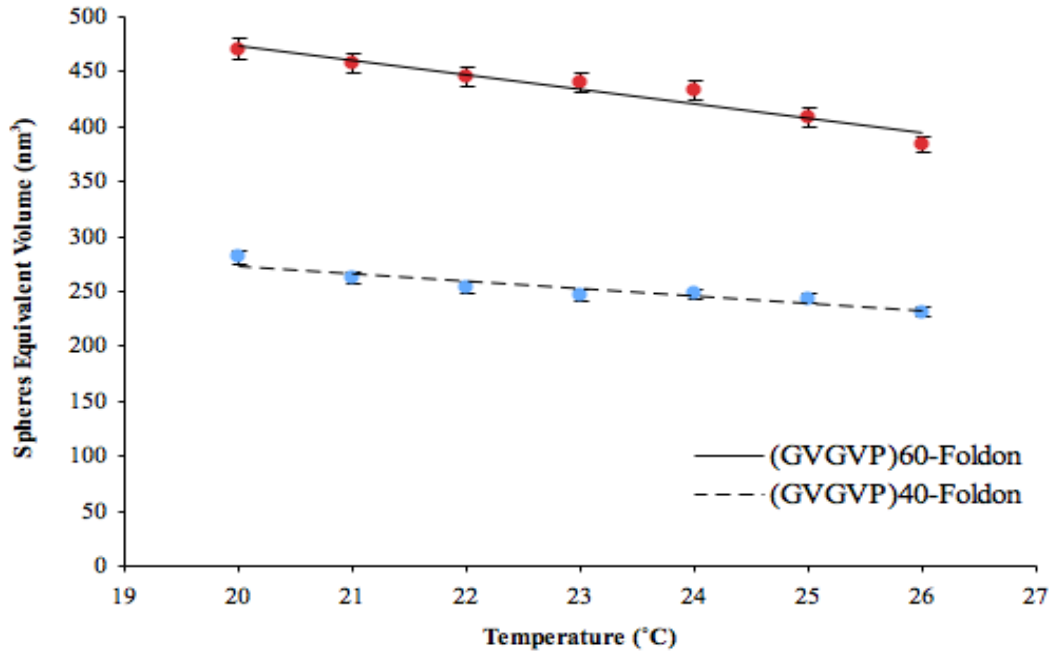


**Figure 3.6: The change of the polymeric sphere equivalent volume of (GVGVP)<sub>40</sub>-foldon and (GVGVP)<sub>60</sub>-foldon as function of the temperature using equation 3.10**

An increase in the temperature causes the polymer coil to become less expanded and the equivalent radius will decrease. As a result the drag force on the polymers will decrease. In other words, the density of the polymer increases as a result of less expanded conformation caused by an increase in the temperature.

### 3.3 Interpretation of Mark-Houwink-Sakurada (MHS) Constants

If we divide equation 3.10 by the concentration and take the limit to zero concentration, a relation between the intrinsic viscosity, the equivalent radius, and the molecular weight of the polymer is obtained.

$$\lim_{c \rightarrow 0} \eta_{\text{specific}}/C = [\eta] = 2.5 N_A (4\pi/3) (R_e^2/M)^{1.5} M^{0.5} \alpha^3 \quad (3.11)$$

The  $R_e$  is the equivalent radius at theta condition, where the solvent is a poor solvent, and  $(R_e^2/M)$  is constant. The scaling of the molecular weight in  $\alpha$ , the expansion of the coil, is dependent many factors such as the solvent, the temperature, and the polymer-solvent system. For example, in a theta solvent or a poor solvent,  $\alpha$  is unity for all molecular weights leaving a constant  $(2.5 N_A (4\pi/3) (R_e^2/M)^{1.5})$  multiplied by the molecular weight raised to the power of 0.5. On the other hand, in non-theta conditions,  $\alpha$  is proportional to molecular weight up to a power of 0.1. This exponent adds up with the exponent in the yellow highlighted term in Equation 3.11, producing values between 0.5 and 0.8.

The expression for the intrinsic viscosity in equation 3.11 can be written in another form known as the Mark-Houwink-Sakurada equation 1.11.

$$\lim_{c \rightarrow 0} \eta_{\text{specific}}/C = [\eta] = \boxed{2.5 N_A (4\pi/3) (R_e^2/M)^{1.5}} \boxed{M^{0.5} \alpha^3} \quad (3.11)$$

$$[\eta] = \boxed{K} \boxed{(M_v)^a} \quad (1.11)$$

Since the intrinsic viscosities are calculated and the molecular weights are known, the logarithm of the intrinsic viscosities can be plotted against the logarithm of the molecular weights according to equation 3.12.

$$\log [\eta] = \log K + a \log M \quad (3.12)$$

The plot will have an intercept of the logarithm of  $K$  and a slope of the constant  $a$  (Figure 3.7). Ideally there would be measurements of additional samples at different molecular weights, but these are currently not available.

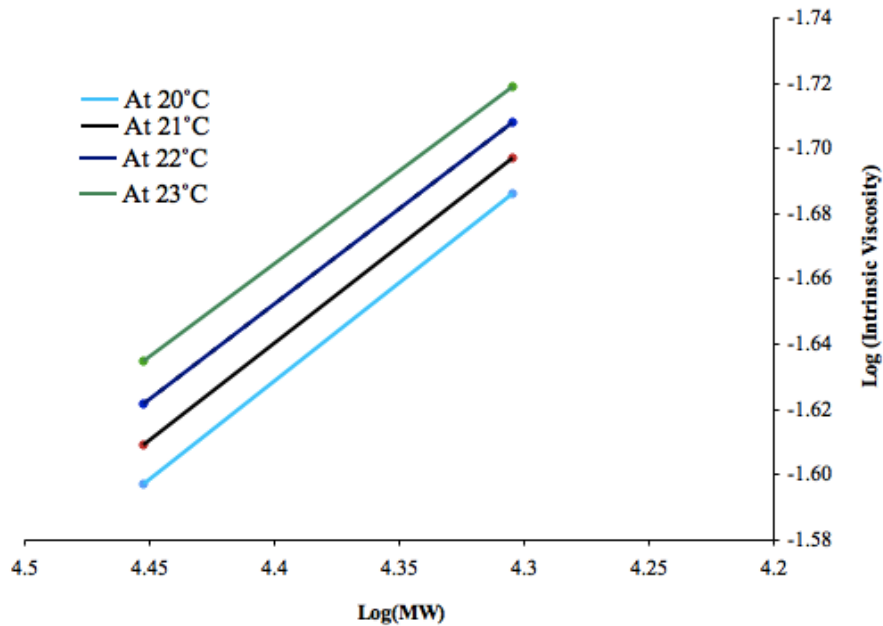


**Figure 3.7: Log  $[\eta]$  of (GVGVP)<sub>60</sub>-foldon versus Log MW of (GVGVP)<sub>40</sub>-foldon and (GVGVP)<sub>60</sub>-foldon with slope of the constant  $a$  and an intercept of log  $K$**

Since the slope is the rise over the run, the constant  $a$  can be calculated according to equation 3.13 by dividing the logarithm of the intrinsic viscosities ratio at one temperature by the logarithm of the molecular weights ratio for the two constructs at the same temperature.

$$a = \text{Log} ([\eta]_1/[\eta]_2) / \text{Log} (M_1/M_2) \quad (3.13)$$

Where the subscript 1 and 2 stands for (GVGVVP)<sub>40</sub>-foldon and (GVGVVP)<sub>60</sub>-foldon respectively. Since the  $a$  constants are calculated for the different temperatures and the molecular weights are known, the MHS equation can be easily solved for the values of  $K$ . The values for  $a$  and  $K$  obtained in this work are specific for (GVGVVP)<sub>n</sub>-foldon - PBS system. The structural change of a polymer in a solvent is represented by the change of the constant  $a$ .

**Table 3.1: Mark-Houwink-Sakurada constants for a novel Elastin-like polypeptide in PBS (Phosphate Buffered Saline) for a range of temperatures between 20°C to 26°C**

Temperature (°C)	$a$	$K$ (cm <sup>3</sup> .mol <sup><math>a</math></sup> /g <sup><math>a+1</math></sup> )
20	0.69	0.020
21	0.67	0.026
22	0.64	0.034
23	0.61	0.044
24	0.58	0.058
25	0.55	0.079
26	0.51	0.108

Conformational changes are inferred from the changes in the values of the constant  $a$  in Table 3.1. The values of the constant  $a$  for (GVGVVP)<sub>n</sub>-foldon - PBS system are decreasing as the temperature is increased. The calculated  $a$  values represent a structural change from a hydrated and expanded random coil collapsing to theta coil according to Table 1.4. This is consistent with the decreasing equivalent volumes observed as the temperature increases.

## CHAPTER IV

### CONCLUSIONS

Models for the efflux time of PBS, the intrinsic viscosity for (GVGVP)<sub>40</sub>-foldon - PBS system, and (GVGVP)<sub>60</sub>-foldon - PBS system as function of temperature were developed from viscosity measurements. The models were utilized to observe the changes in the calculated  $a$  values in the Mark-Houwink-Sakurada equation 1.11. The changes in the values of  $a$  indicate conformational changes of the ELPs as a function of temperature. The values of  $a$  varied from 0.69 at 21°C, indicating an expanded coil conformation, to 0.51 at 26°C, indicating a less expanded theta coil. This is consistent with the decrease in the volume of the coil with increasing temperature calculated from intrinsic viscosity measurements.

There were two limitations on the viscosity measurements in this project. First, the viscosity measurements at low concentrations could not be obtained because of the increase in error at lower concentrations. When the concentration decreases, the value of the specific viscosity gets closer to zero and therefore increasing the error value. Second, the polymer aggregates at  $T_i$  and phase separate and therefore the viscosity measurements

are meaningless after the occurrence of phase separation. Future work might investigate the possibility of eliminating the limitations imposed on the system studied in this project by comparing it to large linear ELPs, which will have larger specific viscosities. Other constructs that do not aggregate but rather form micelles at  $T_i$  might also be studied. The role of salt concentration and pH on the structure of these constructs might also be investigated.

## BIBLIOGRAPHY

- [1] Meyer, Dan E. and Ashutosh Chilkoti. "Genetically Encoded Synthesis of Protein-Based Polymers with Precisely Specified Molecular Weight and Sequence by Recursive Directional Ligation: Examples from the Elastin-like Polypeptide System." *Biomacromolecules* 3.2 (2002), 357-367.
- [2] Urry, Dan W. "Physical Chemistry of Biological Free Energy Transduction As Demonstrated by Elastic Protein-Based Polymers." *Journal of Physical Chemistry B* 101.51 (1997), 11007-11028.
- [3] Nauš, J. "Spectroscopic Methods for Determining Protein Structure in Solution." *Biologia Plantarum* 38.4 (1996), 620.
- [4] Getie, M., C.E.H. Schmelzer, and R.H.H. Neubert. "Characterization of peptides resulting from digestion of human skin elastin with elastase." *Proteins: Structure, Function, and Bioinformatics* 61.3 (2005), 649 - 657.
- [5] Lee, Jonghwi, Christopher W. Macosko, and Dan W. Urry. "Mechanical Properties of Cross-Linked Synthetic Elastomeric Polypentapeptides." *Macromolecules* 34.17 (2001), 5968-5974
- [6] Debelle L. Tamburro AM. "Elastin: molecular description and function." *International Journal of Biochemistry & Cell Biology* 31(1999), 261-272.
- [7] Green, Ellen, Richard Ellis, and Peter Winlove. "The molecular structure and physical properties of elastin fibers as revealed by Raman microspectroscopy." *Biopolymers* 89.11 (2008), 931 - 940.
- [8] Petsko, Gregory A., and Dagmar Ringe. *Protein Structure and Function*. London: New Science, 2004.



- [9] Vrhovski, Bernadette, Sacha Jensen, and Anthony S. Weiss. "Coacervation Characteristics of Recombinant Human Tropoelastin." *European Journal of Biochemistry* 250.1 (1997), 92-98.
- [10] Liu, W., Dreher, M. R., Furgeson, D. Y., Peixoto, K. V., Yuan, H., Zalutsky, M. R., and Ashutosh Chilkoti "Tumor accumulation, degradation and pharmacokinetics of elastin-like polypeptides in nude mice." *Journal of Controlled Release* 116.2 (2006), 170-178.
- [11] Chilkoti, Ashutosh, Trine Christensen, and J Andrew MacKay. "Stimulus responsive elastin biopolymers: applications in medicine and biotechnology." *Current Opinion in Chemical Biology* 10.6 (2006), 652-657.
- [12] Van Vlierberghe, S., P. Dubruel, and E. Schacht. "Biopolymer-Based Hydrogels As Scaffolds for Tissue Engineering Applications: A Review." *Biomacromolecules* 12.5 (2011), 1387-1408.
- [13] Laromaine, A., Koh, L., Murugesan, M., Ulijn, R. V., and Stevens M. "Protease-Triggered Dispersion of Nanoparticle Assemblies." *Journal of the American Chemical Society* 129.14 (2007), 4156-4157.
- [14] Chow, Dominic, Nunalee, M., Lim, D. W., Simnick, A. J., and Ashutosh Chilkoti. "Peptide-based biopolymers in biomedicine and biotechnology." *Materials Science & Engineering R* 62.4 (2008), 125-155.
- [15] Paiva, L. R. and M. L. Martins. "A multiscale model to evaluate the efficacy of anticancer therapies based on chimeric polypeptide nanoparticles." *Applied Physics Letters* 98.5 (2011), 053703-053703-3.

- [16] Adams, Samuel B., Shamji, Mohammed F., Nettles, Dana L., Hwang, Priscilla, and Lori Setton. "Sustained release of antibiotics from injectable and thermally responsive polypeptide depots." *Journal of Biomedical Materials Research Part B: Applied Biomaterials* 90B.1 (2009), 67 - 74.
- [17] Sorg, Brian, Peltz, Cathryn D, Klitzman, Bruce, and Mark Dewhirst. "Method for improved accuracy in endogenous urea recovery marker calibrations for microdialysis in tumors." *Journal of Pharmacological and Toxicological Methods* 52.3 (2005), 341-349.
- [18] Temming, Kai, Schiffelers, Raymond, Molema, Grietje, and Robbert J. Kok. "RGD-based strategies for selective delivery of therapeutics and imaging agents to the tumor vasculature." *Drug Resistance Updates* 8.6 (2005), 381-402.
- [19] Betre, Helawe, Liu, Wenge, Zalutsky, Michael R., Chilkoti, Ashutosh, Kraus, Virginia, and Lori Setton. "A thermally responsive biopolymer for intra-articular drug delivery." *Journal of Controlled Release* 115.2 (2006), 175-182.
- [20] Betre, Helawe, Liu, Wenge, Zalutsky, Michael R., Chilkoti, Ashutosh, Kraus, Virginia, and Lori Setton. "In vitro skin penetration of dazmegrel delivered with a bioelastic matrix." *International Journal of Pharmaceutics* 271.1-2 (2004), 301-303.
- [21] Kemppainen, Barbara, Urry, Dan W., Luan, Chi-Xiang, Xu, Jie, Swaim, Steven, and Saryu Goel. "Characterization of a Genetically Engineered Elastin-like Polypeptide for Cartilaginous Tissue Repair." *Biomacromolecules* 3.5 (2002), 910-916.
- [22] Kumar, Ashok, Srivastava, Akshay, Galaev, Igor Yu, and Bo Mattiasson. "Smart polymers: Physical forms and bioengineering applications." *Progress in Polymer Science* 32.10 (2007), 1205-1237.

- [23] Urry, D. W, Hugel T, Seitz M, Gaub H. E, Sheiba L, Dea J, Xu J, and Parker T. "Elastin: a representative ideal protein elastomer." *Philosophical Transactions: Biological Sciences* 357.1418 (2002), 169-184.
- [24] Li, Bin and Valerie Daggett. "The molecular basis of the temperature- and pH-induced conformational transitions in elastin-based peptides." *Biopolymers* 68.1 (2003), 121 - 129.
- [25] Reguera, Javier, Urry, Dan W., Parker, Timothy M., McPherson, David T., and Carlos Rodríguez-Cabello. "Effect of NaCl on the Exothermic and Endothermic Components of the Inverse Temperature Transition of a Model Elastin-like Polymer." *Biomacromolecules* 8.2 (2007), 354-358.
- [26] Nuhn, Harald and Harm-Anton Klok. "Secondary Structure Formation and LCST Behavior of Short Elastin-Like Peptides." *Biomacromolecules* 9.10 (2008), 2755-2763.
- [27] Yamaoka, Tetsuji, Tamura, Takumi, Seto, Yuuki, Tada, Tomoko, Kunugi, Shigeru, and David Tirrell. "Mechanism for the Phase Transition of a Genetically Engineered Elastin Model Peptide (VPGIG)<sub>40</sub> in Aqueous Solution." *Biomacromolecules* 4.6 (2003), 1680-1685.
- [28] Cho, Younhee, Zhang, Yanjie, Christensen, Trine, Sagle, Laura B., Chilkoti, Ashutosh, and Paul S. Cremer. "Effects of Hofmeister Anions on the Phase Transition Temperature of Elastin-like Polypeptides." *Journal of Physical Chemistry B* 112.44 (2008), 13765-13771.
- [29] Ghoorchian, Ali, James T. Cole, and Nolan B. Holland. "Thermoreversible Micelle Formation Using a Three-Armed Star Elastin-like Polypeptide." *Macromolecules* 43.9 (2010), 4340-4345.

- [30] Fong, Baley A., Wan-Yi Wu, and David W. Wood. "Optimization of ELP-intein mediated protein purification by salt substitution." *Protein Expression and Purification* 66.2 (2009), 198-202.
- [31] Gualrdia, Elvira, Ioannis Skarmoutsos, and Marco Masia. "On Ion and Molecular Polarization of Halides in Water." *Journal of Chemical Theory and Computation* 5.6 (2009), 1449-1453.
- [32] MacKay, J. Andrew, Callahan, Daniel J., FitzGerald, Kelly N., and Ashutosh Chilkoti. "Quantitative Model of the Phase Behavior of Recombinant pH-Responsive Elastin-Like Polypeptides." *Biomacromolecules* 11.11 (2010), 2873-2879.
- [33] Meyer, Dan E. and Ashutosh Chilkoti. "Quantification of the Effects of Chain Length and Concentration on the Thermal Behavior of Elastin-like Polypeptides." *Biomacromolecules* 5.3 (2004), 846-851.
- [34] Baldwin, Robert L. "The nature of protein folding pathways: The classical versus the new view." *Journal of Biomolecular NMR* 5.2 (1995), 103 - 109.
- [35] Urry, Dan W. "Entropic elastic processes in protein mechanisms. I. Elastic structure due to an inverse temperature transition and elasticity due to internal chain dynamics." *Journal of Protein Chemistry* 7.1 (1988), 1 – 34.
- [36] Urry, Dan W. "Entropic elastic processes in protein mechanisms. II. Simple (passive) and coupled (active) development of elastic forces." *Journal of Protein Chemistry* 7.2 (1988), 81 - 114.
- [37] Nicolini, C., Ravindra, R., Ludolph, B., and Winter R. "Characterization of the Temperature- and Pressure-Induced Inverse and Reentrant Transition of the Minimum

Elastin-Like Polypeptide GVG(VPGVG) by DSC, PPC, CD, and FT-IR Spectroscopy." *Biophysical Journal* 86.3 (2004), 1385-1392.

[38] Knab, Joseph, Jing-Yin Chen, and Andrea Markelz. "Hydration Dependence of Conformational Dielectric Relaxation of Lysozyme." *Biophysical Journal* 90.7 (2006), 2576-2581.

[39] Krukau, Aliaksei, Ivan Brovchenko, and Alfons Geiger. "Temperature-Induced Conformational Transition of a Model Elastin-like Peptide GVG(VPGVG)<sub>3</sub> in Water." *Biomacromolecules* 8.7 (2007), 2196-2202.

[40] Li, Bin, Alonso, Darwin O. V., Bennion, Brian J., and Valerie Daggett. "Hydrophobic Hydration is an Important Source of Elasticity in Elastin-Based Biopolymers." *Journal of the American Chemical Society* 123.48 (2001), 11991-11998.

[41] Lee, Jonghwi, Christopher MacOsco, and Dan Urry. "Phase transition and elasticity of protein-based hydrogels." *Journal of Biomaterials Science, Polymer Edition* 12.2 (2001), 229-242.

[42] Tao, Yizhi, Strelkov, Sergei, Mesyanzhinov, Vadim, and Michael G. Rossmann. "Structure of bacteriophage T4 fibritin: a segmented coiled coil and the role of the C-terminal domain." *Structure* 5.6 (1997), 789-798.

[43] Efimov, Vladimir P., Nepluev, Igor V., Sobolev, Boris N., Zurabishvili, Timur G., Schulthess, Therese, Lustig, Ariel, Engel, Juergen, Haener, Markus, Aebi, Ueli, Venyaminov, Sergey Yu., Potekhin, Sergey A., and Vadim V. Mesyanzhinov. "Fibritin Encoded by Bacteriophage T4 Gene *wac* has a Parallel Triple-stranded  $\alpha$ -Helical Coiled-coil Structure." *Journal of Molecular Biology* 242.4 (1994), 470 - 486.

- [44] Pellarin, Riccardo and Amedeo Caflisch. "Interpreting the Aggregation Kinetics of Amyloid Peptides." *Journal of Molecular Biology* 360.4 (2006), 882-892.
- [45] Pappu, Rohit V., Wang, Xiaoling, Vitalis, Andreas, and Scott L. Crick. "A polymer physics perspective on driving forces and mechanisms for protein aggregation." *Archives of Biochemistry and Biophysics* 469.1 (2008), 132-141.
- [46] Kurková, Dana, Kříž, Jaroslav, Rodríguez-Cabello, José Carlos, and Francisco Javier Arias. "NMR study of the cooperative behavior of thermotropic model polypeptides." *Polymer International* 56.2 (2007), 186 - 194.
- [47] Graves, Rachel, Baer, Marcel, Schreiner, Eduard, Stoll, Raphael, and Dominik Marx. "Conformational Dynamics of Minimal Elastin-Like Polypeptides: The Role of Proline Revealed by Molecular Dynamics and Nuclear Magnetic Resonance." *ChemPhysChem* 9.18 (2008), 2759-2765.
- [48] Dybal, Jiří, Schmidt, Pavel, Kříž, Jaroslav, Kurková, Dana, Rodríguez-Cabello, José Carlos, and Matilde Alonso. "Role of hydration in the phase transition of polypeptides investigated by NMR and Raman spectroscopy." *Macromolecular Symposia* 205.1 (2004), 143 - 150.
- [49] Boichichio, Brigida, Antonietta Pepe, and Antonio M. Tamburro. "Investigating by CD the molecular mechanism of elasticity of elastomeric proteins." *Chirality* 20.9 (2008), 985 - 994.
- [50] Tamburro, Antonio Mario, Lorusso, Marina, Ibris, Neluta, Pepe, Antonietta, and Brigida Boichichio. "Investigating by circular dichroism some amyloidogenic elastin-derived polypeptides ." *Chirality* 22.1E (2010), E56-E66.

- [51] Sperling, L. H. *Introduction to Physical Polymer Science*. Hoboken, NJ: Wiley, **2006**.
- [52] Christensen, Douglas A. *Introduction to Biomedical Engineering: Biomechanics and Bioelectricity*. [San Rafael, CA]: Morgan & Claypool, **2009**.
- [53] Eugene, Frederick. *Smithsonian Physical Tables*. South Carolina: BiblioLife, **2009**.

## **APPENDICES**



## APPENDIX A

### (Viscometer Constant Calibration)

The constant for the viscometer was verified through comparing the literature and the experimental measurements and it was calculated to be 0.001909 cSt/s.

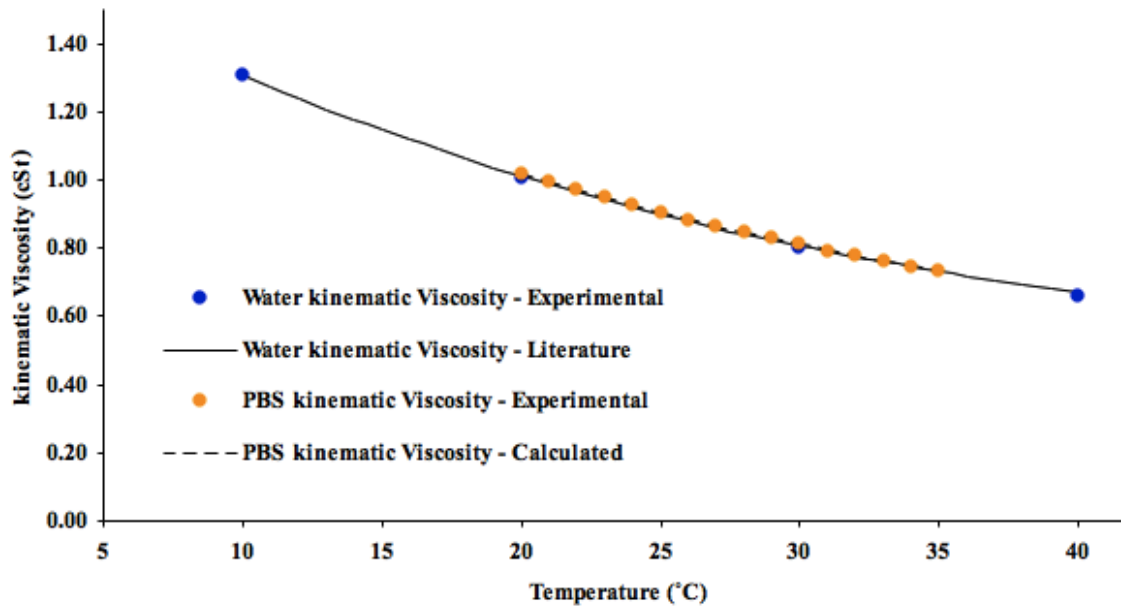


**Figure A.1: Viscosity of water and PBS solvent**

A small deviation for the experimental kinematics viscosity of water from literature values can be observed above. Since the PBS contains 98% water, its viscosity was close to water [53].

## APPENDIX B

### (Intrinsic Viscosity Graphs)

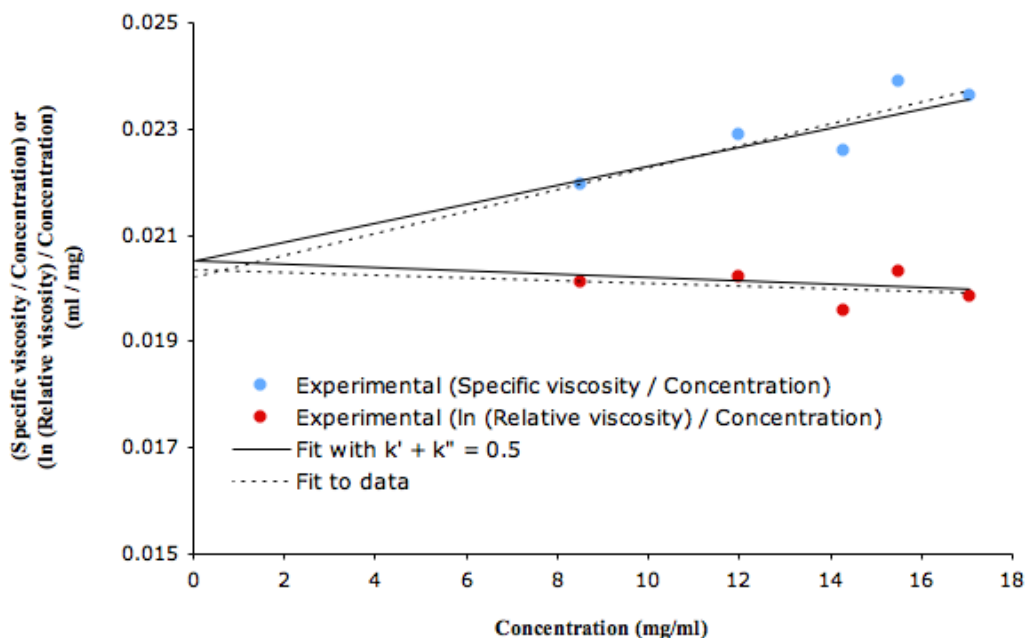


**Figure B.1: Plot of  $\eta_{\text{specific}}/c$  versus  $c$  and also  $(\text{Ln } \eta_{\text{relative}})/c$  versus  $c$  for (GVGVVP)<sub>40</sub>-foldon at 20°C extrapolated to zero concentration to find an intrinsic viscosity of 0.0210 ml/mg with a standard deviation  $\pm 3\%$ .**

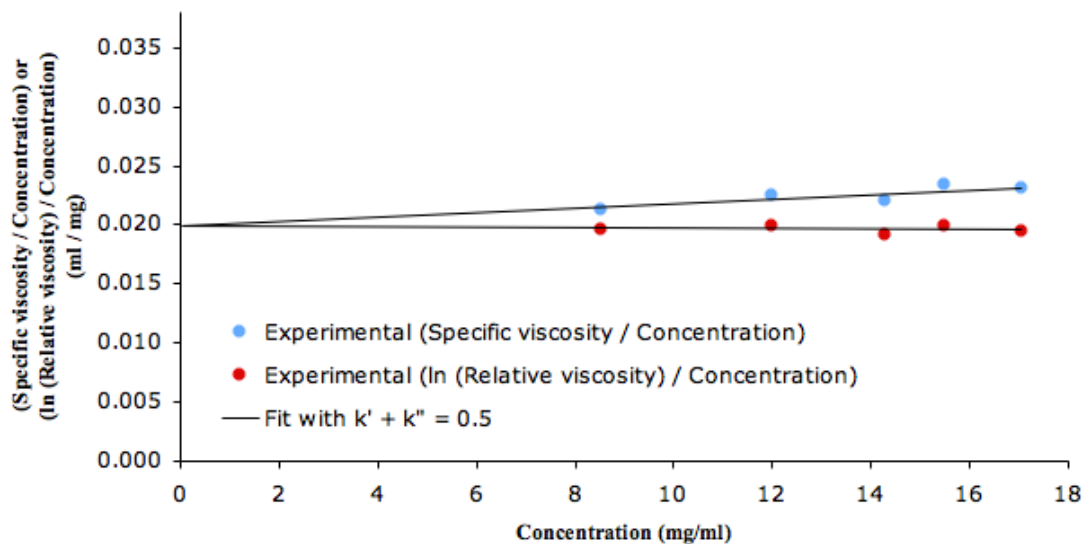


**Figure B.2: Plot of  $\eta_{\text{specific}}/c$  versus  $c$  and also  $(\text{Ln } \eta_{\text{relative}})/c$  versus  $c$  for (GVGVVP)<sub>40</sub>-foldon at 21°C extrapolated to zero concentration to find an intrinsic viscosity of 0.0196 ml/mg with a standard deviation  $\pm 2\%$ .**

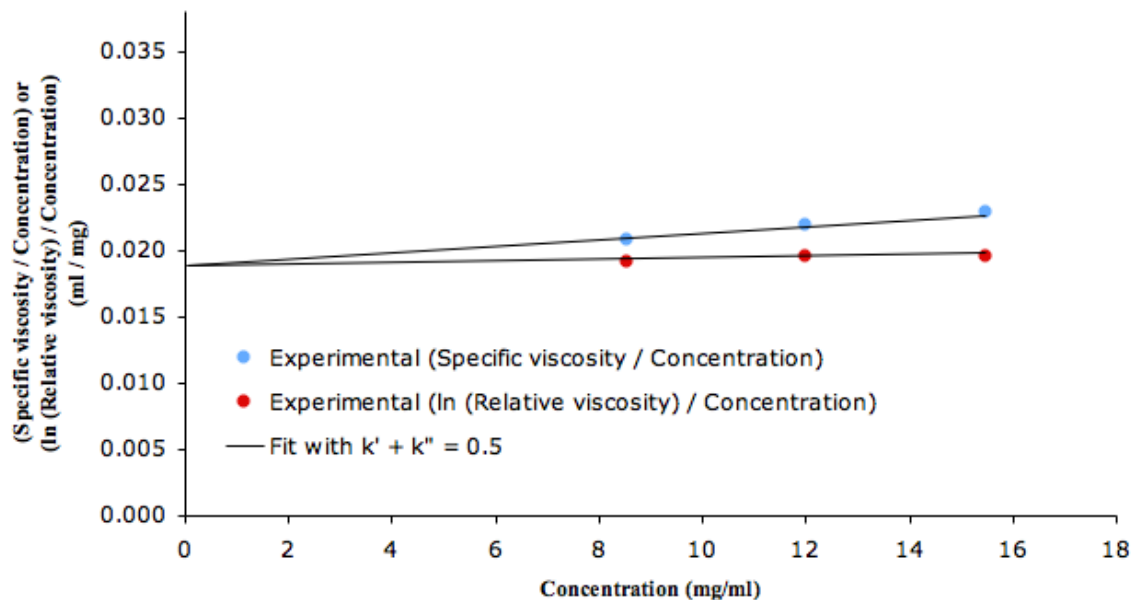


**Figure B.3: Plot of  $\eta_{\text{specific}}/c$  versus  $c$  and also  $(\text{Ln } \eta_{\text{relative}})/c$  versus  $c$  for (GVGVP)<sub>40</sub>-foldon at 22°C extrapolated to zero concentration to find an intrinsic viscosity of 0.0196 ml/mg with a standard deviation  $\pm 2\%$ .**

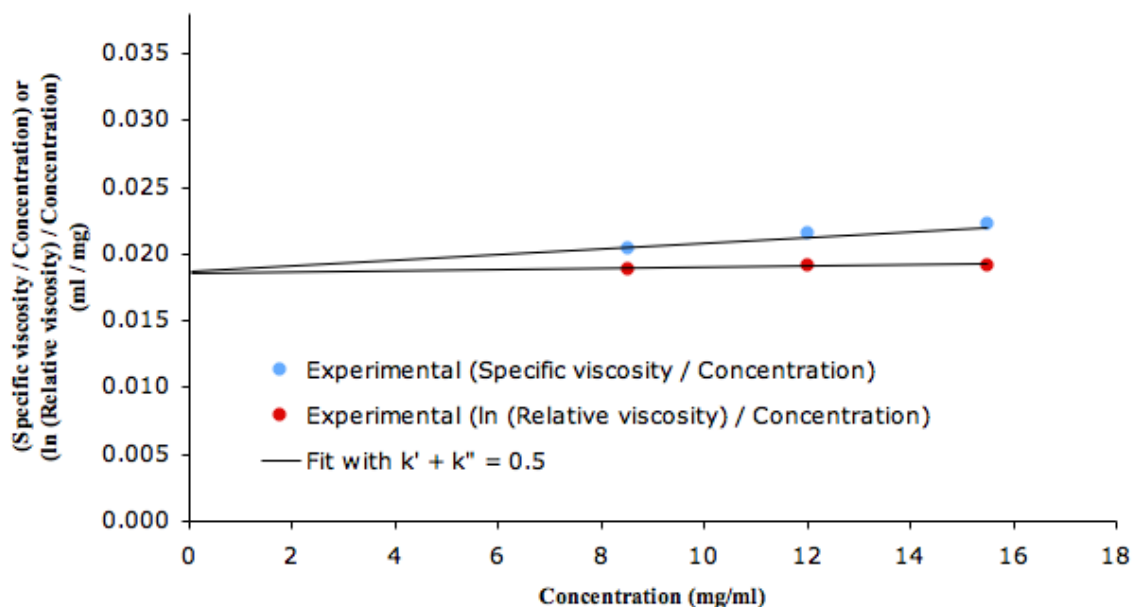


**Figure B.4: Plot of  $\eta_{\text{specific}}/c$  versus  $c$  and also  $(\text{Ln } \eta_{\text{relative}})/c$  versus  $c$  for (GVGVP)<sub>40</sub>-foldon at 23°C extrapolated to zero concentration to find an intrinsic viscosity of 0.0184 ml/mg with a standard deviation  $\pm 2\%$ .**

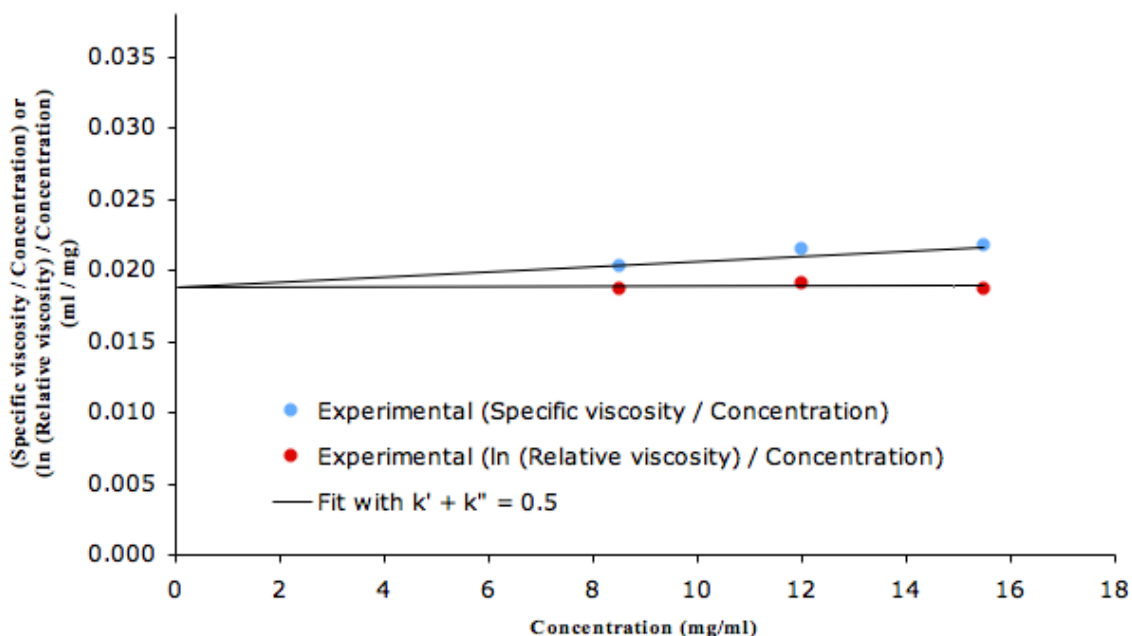


**Figure B.5:** Plot of  $\eta_{\text{specific}}/c$  versus  $c$  and also  $(\text{Ln } \eta_{\text{relative}})/c$  versus  $c$  for (GVGVP)<sub>40</sub>-foldon at 24°C extrapolated to zero concentration to find an intrinsic viscosity of 0.0185 ml/mg with a standard deviation  $\pm 2\%$ .

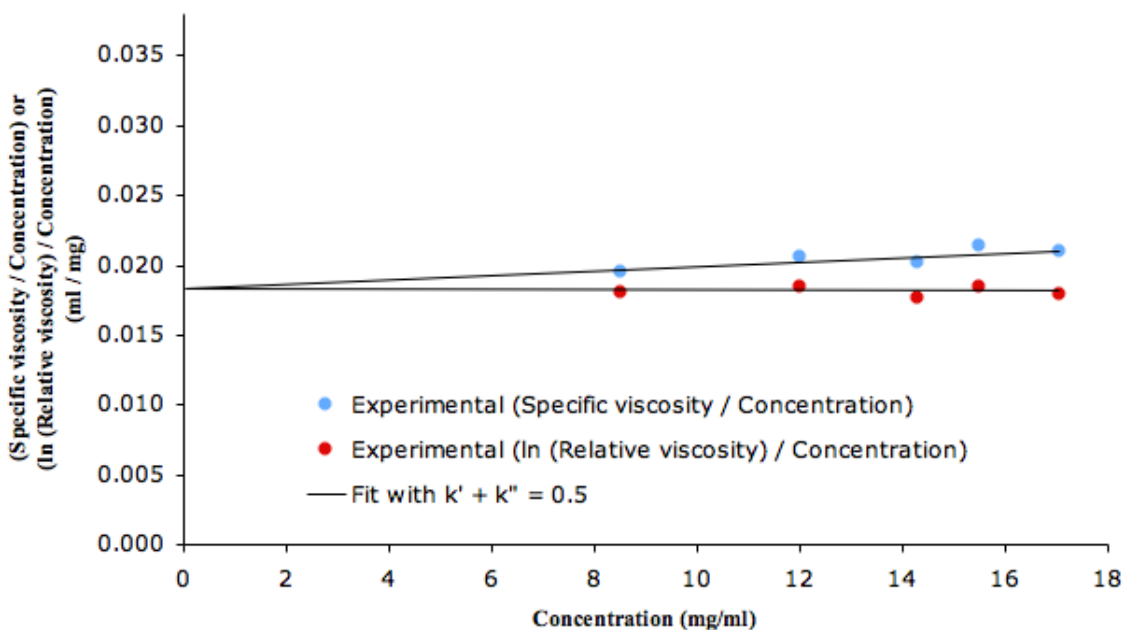


**Figure B.6:** Plot of  $\eta_{\text{specific}}/c$  versus  $c$  and also  $(\text{Ln } \eta_{\text{relative}})/c$  versus  $c$  for (GVGVP)<sub>40</sub>-foldon at 25°C extrapolated to zero concentration to find an intrinsic viscosity of 0.0182 ml/mg with a standard deviation  $\pm 2\%$ .

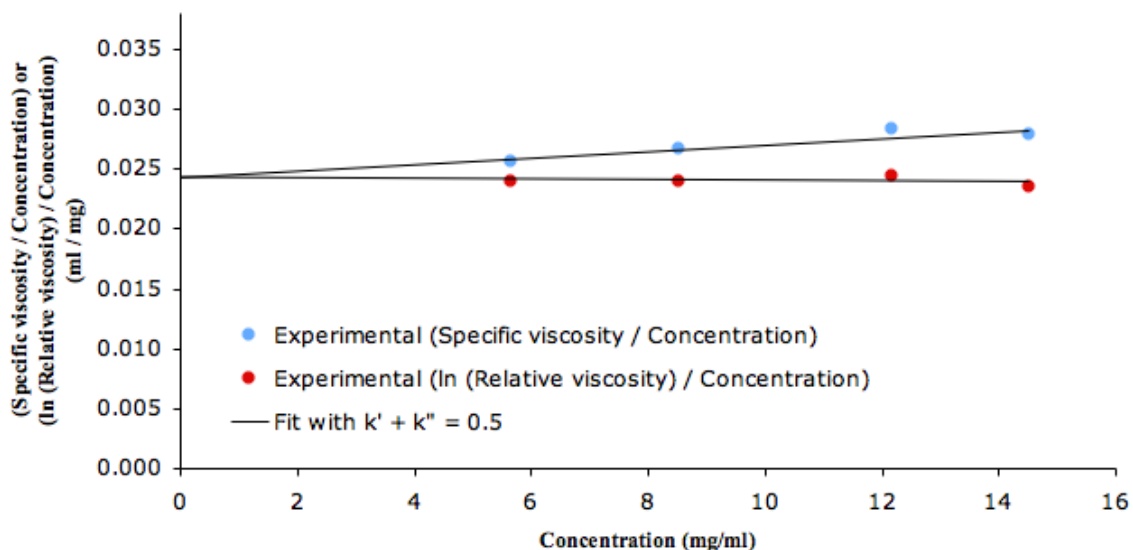


**Figure B.7:** Plot of  $\eta_{\text{specific}}/c$  versus  $c$  and also  $(\text{Ln } \eta_{\text{relative}})/c$  versus  $c$  for (GVGVP)<sub>60</sub>-foldon at 20°C extrapolated to zero concentration to find an intrinsic viscosity of 0.0250 ml/mg with a standard deviation  $\pm 3\%$ .

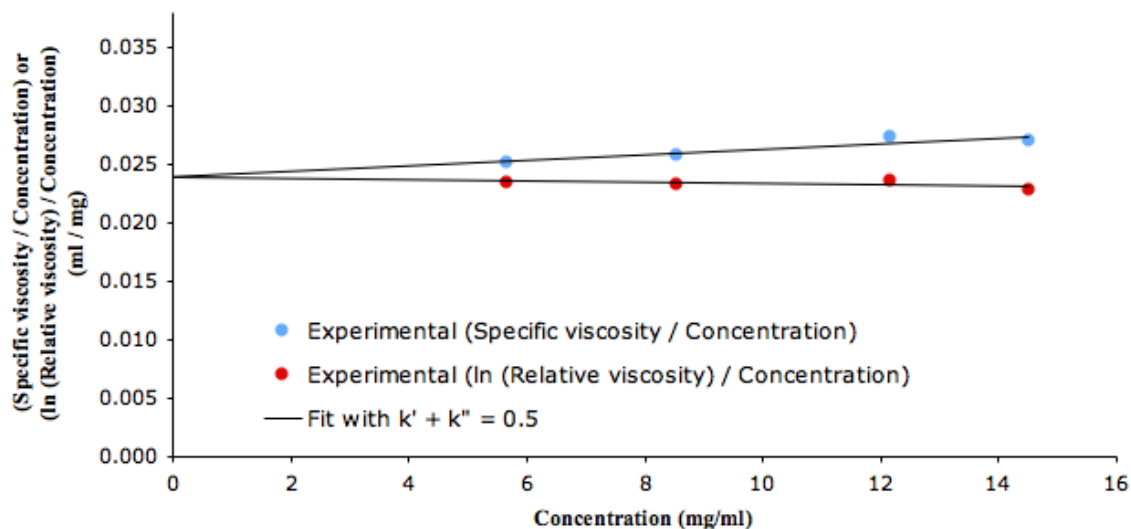


**Figure B.8:** Plot of  $\eta_{\text{specific}}/c$  versus  $c$  and also  $(\text{Ln } \eta_{\text{relative}})/c$  versus  $c$  for (GVGVP)<sub>60</sub>-foldon at 21°C extrapolated to zero concentration to find an intrinsic viscosity of 0.0243 ml/mg with a standard deviation  $\pm 2\%$ .

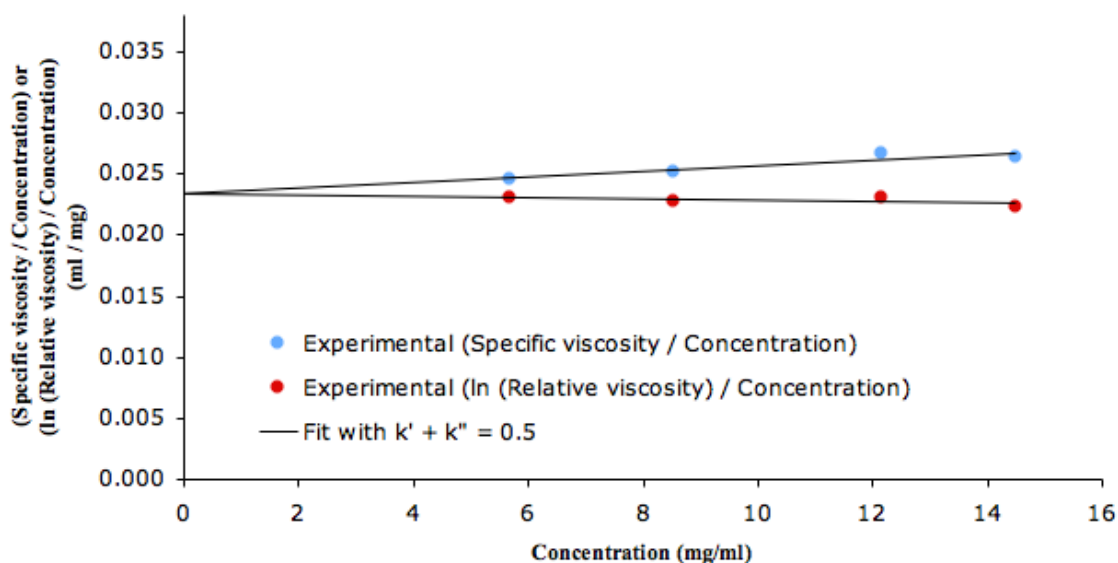


**Figure B.9:** Plot of  $\eta_{\text{specific}}/c$  versus  $c$  and also  $(\text{Ln } \eta_{\text{relative}})/c$  versus  $c$  for (GVGV P)<sub>60</sub>-foldon at 22°C extrapolated to zero concentration to find an intrinsic viscosity of 0.0237 ml/mg with a standard deviation  $\pm 2\%$ .

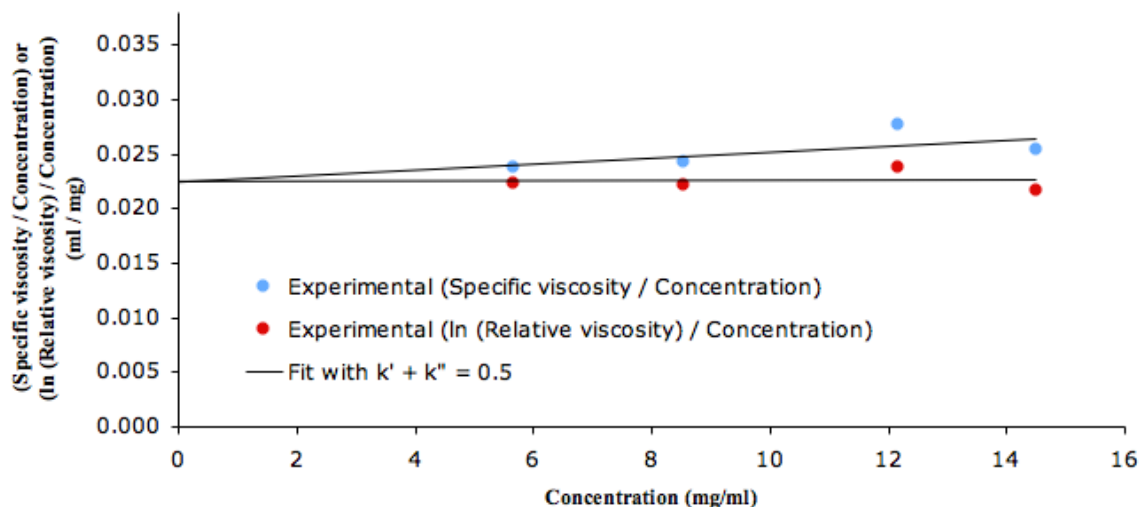


**Figure B.10:** Plot of  $\eta_{\text{specific}}/c$  versus  $c$  and also  $(\text{Ln } \eta_{\text{relative}})/c$  versus  $c$  for (GVGV P)<sub>60</sub>-foldon at 23°C extrapolated to zero concentration to find an intrinsic viscosity of 0.0234 ml/mg with a standard deviation  $\pm 5\%$ .

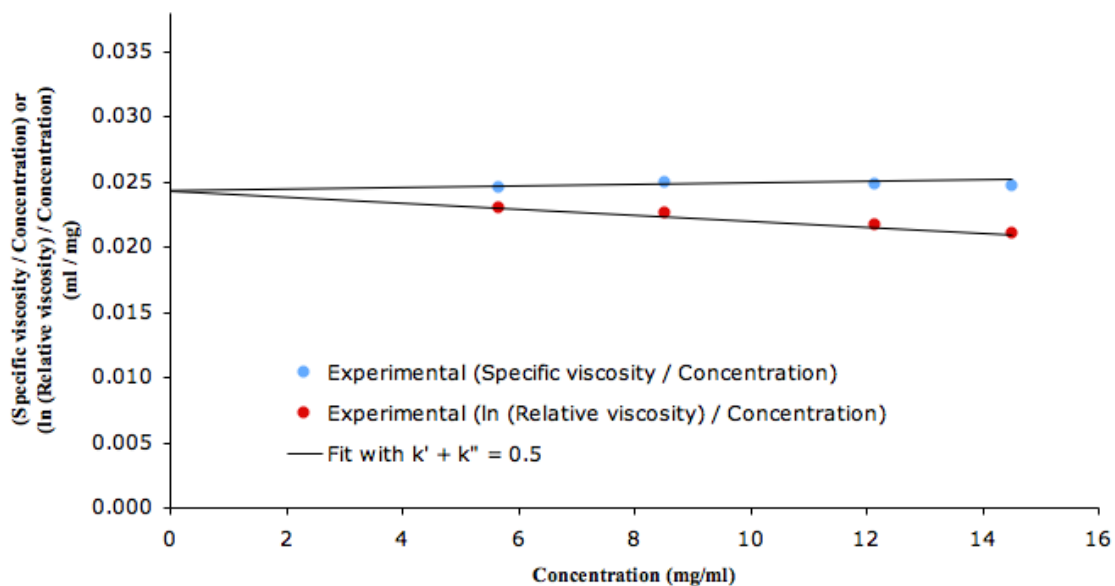


Figure B.11: Plot of  $\eta_{\text{specific}}/c$  versus  $c$  and also  $(\ln \eta_{\text{relative}})/c$  versus  $c$  for (GVGVP)<sub>60</sub>-foldon at 24°C extrapolated to zero concentration to find an intrinsic viscosity of 0.0230 ml/mg with a standard deviation  $\pm 3\%$ .

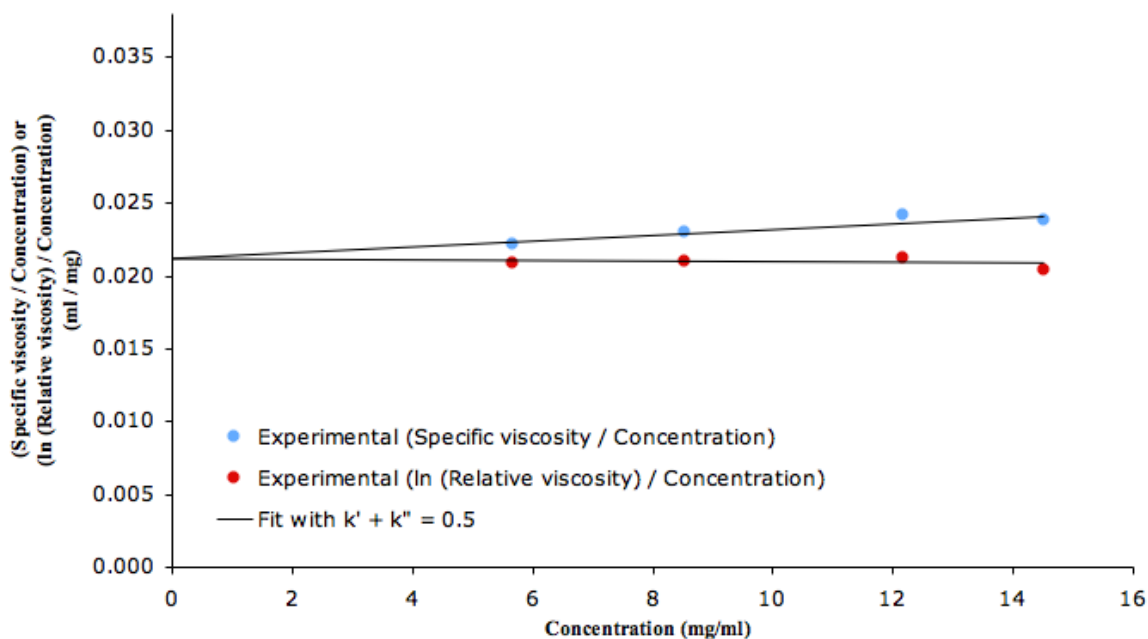
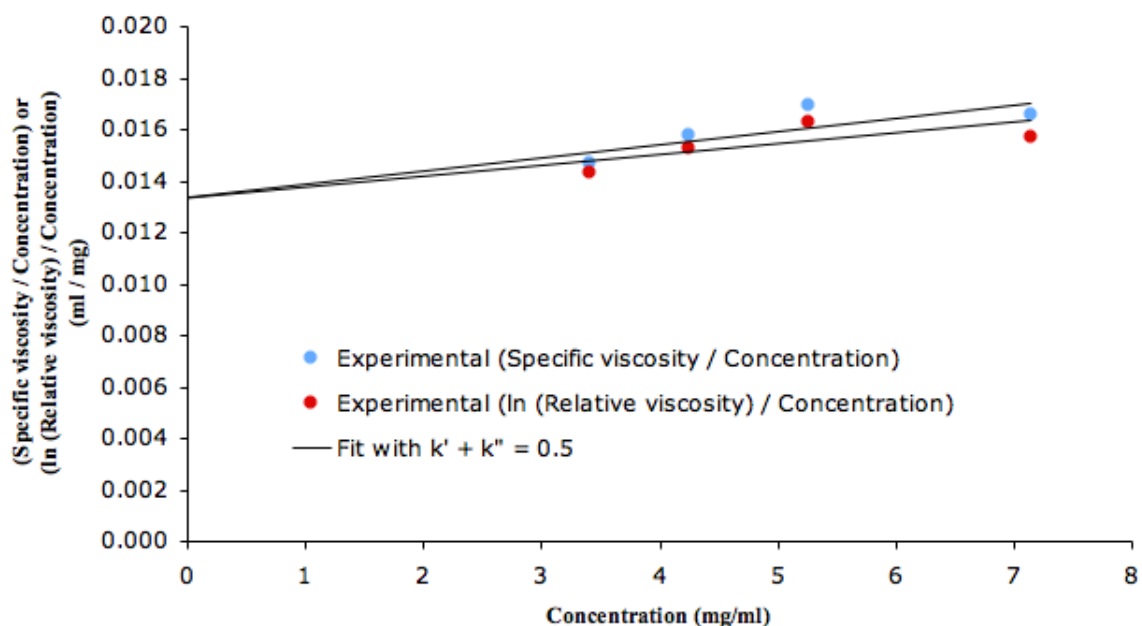
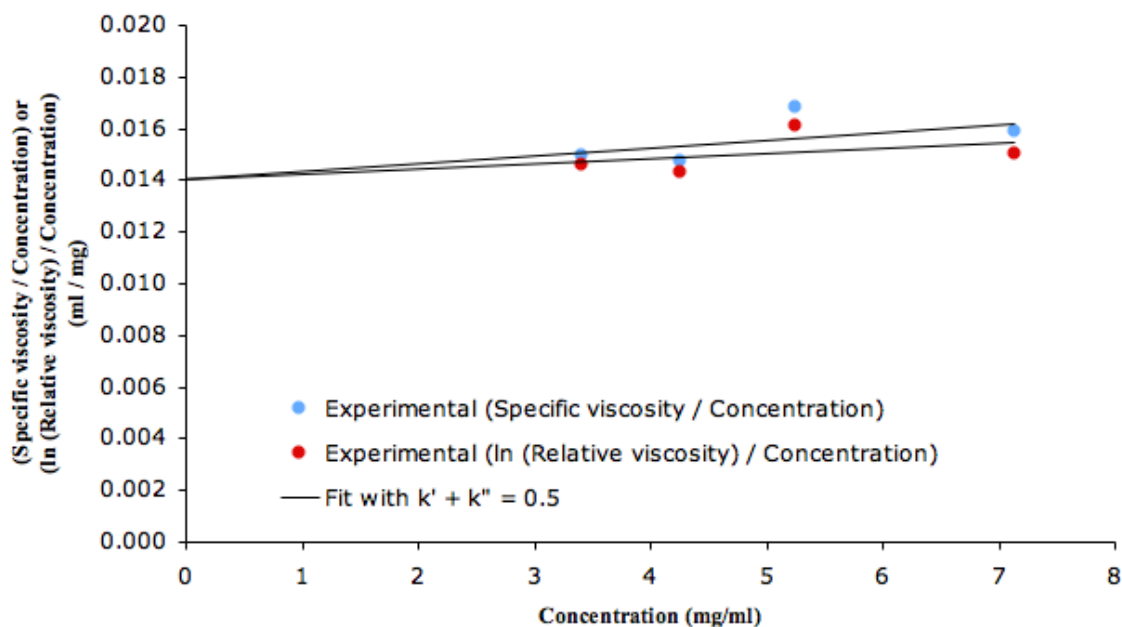


Figure B.12: Plot of  $\eta_{\text{specific}}/c$  versus  $c$  and also  $(\ln \eta_{\text{relative}})/c$  versus  $c$  for (GVGVP)<sub>60</sub>-foldon at 25°C extrapolated to zero concentration to find an intrinsic viscosity of 0.0217 ml/mg with a standard deviation  $\pm 2\%$ .



**Figure B.13:** Plot of  $\eta_{\text{specific}}/c$  versus  $c$  and also  $(\text{Ln } \eta_{\text{relative}})/c$  versus  $c$  for (GVGVP)<sub>40</sub> at 25°C extrapolated to zero concentration to find an intrinsic viscosity of 0.0139 ml/mg with a standard deviation  $\pm 10\%$ .



**Figure B.14:** Plot of  $\eta_{\text{specific}}/c$  versus  $c$  and also  $(\text{Ln } \eta_{\text{relative}})/c$  versus  $c$  for (GVGVP)<sub>40</sub> at 30°C extrapolated to zero concentration to find an intrinsic viscosity of 0.0143 ml/mg with a standard deviation  $\pm 6\%$ .



## APPENDIX C

### (Viscosity Measurements Procedure)

- Make sure the Cannon-Ubbelohde Semi-Micro viscometer (Figure 2.2) is cleaned with distilled water, dried with vacuumed air, and placed in the viscometer bath (Figure 2.1).

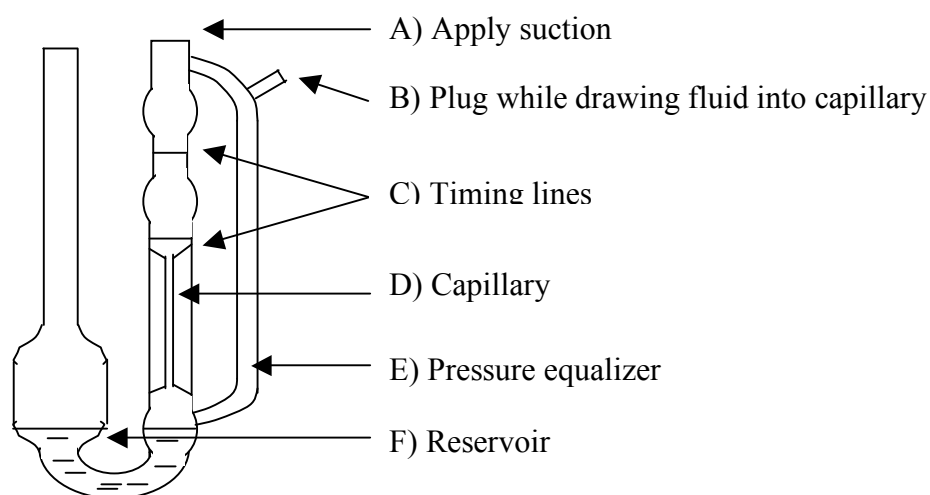


**Figure 2.2: Schematic drawing of the cannon capillary viscometer**

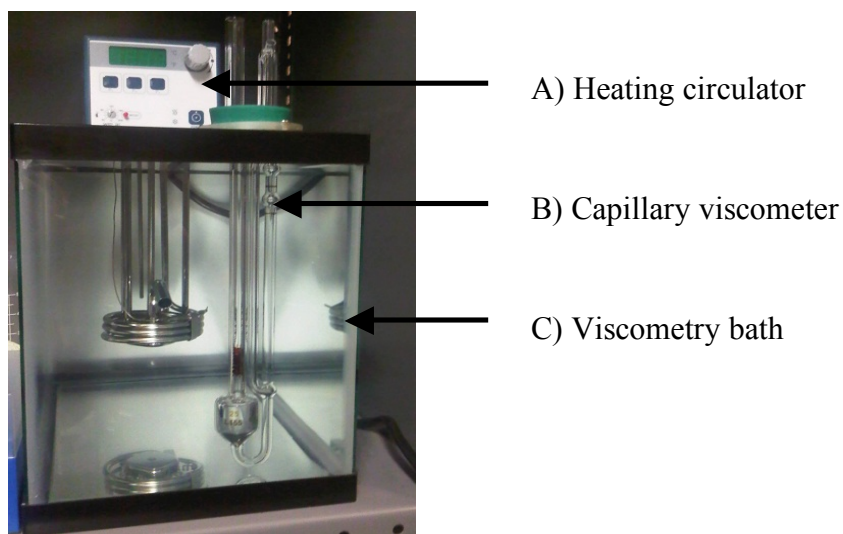


**Figure 2.1: Viscometry bath with a heating circulator**

- Since the heating circulator will not work below ambient temperature, the viscometer bath is placed in a cold room at 5°C to facilitate viscosity measurements below the ambient temperature.
- A video recorder is turned on and placed next to the viscometer bath wall and aligned with the upper timing line on the viscometer.
- A known amount of water or solvent or ELP, between 1 ml and 2.5 ml, is loaded into the reservoir of the viscometer.
- The heating circulator in the viscometer bath is set to a desired temperature.
- Enough time is given to let the temperature of the bath reaches equilibrium, around 10 minutes.
- Once the targeted temperature is reached and it is not fluctuating, the recording button on the video recorder is turned on.
- Suction is applied at point A in Figure 2.2 while point B is plugged with the experimenter thumb.
- After the solution passes above the upper timing line, the opening of B is unplugged first then the suction is released.
- Make sure the video recorder is aligned with the upper timing line. Once the meniscus of the solution in the capillary reaches the upper timing line, start the stopwatch.
- After the solution passes below the upper timing line, align the video recorder with the bottom timing line and speak loudly identifying the type of solution you

are measuring, the concentration, the temperature, and any other important comments that you want to save on the recorder.

- Stop the stopwatch once the meniscus of the solution in the capillary reaches the bottom timing line.
- Record the efflux time on the stopwatch.
- Repeat the steps above to take a second measurement to confirm the accuracy of the data.
- If the efflux times for the two measurements are not in agreement, repeat the steps for a third measurement. Fourth measurement might also be conducted if necessary.
- Then, stop the recording. Note that the video recorder is still on but not recording after stopping or pausing the recording function.
- Change the temperature on the heating circulator to another desired value and wait for the temperature in the viscometer bath to reach equilibrium.
- Then, repeat the same procedure.
- Obtain measurements for the desired range of temperature.
- After the viscosity measurements are obtained for the desired range of temperatures, the concentration of the solution can be diluted in the viscometer and new measurements can be taken.
- After all measurements are taken, the video recorder and the heating circulator are turned off. Then, the solution is emptied in a tube and the viscometer is cleaned with distilled water and dried with vacuumed air.

- Finally, the video recorder tapes are analyzed to obtain the recorded timing for each measurement.